

Entropic Forces in Rotaxane-Based Daisy Chains: Toward Tunable Nanomechanical Systems

Gaétan Sanchez,^{1,2} Claudia Binetti,^{1,2} Giuseppe Florio,^{2,3} Nicola M. Pugno,^{4,5} Giuseppe Puglisi,² and Stefano Giordano*¹

¹University of Lille, CNRS, Centrale Lille, Univ. Polytechnique Hauts-de-France, UMR 8520 - IEMN - Institut d'Électronique, de Microélectronique et de Nanotechnologie, Lille, F-59000, France

²Department of Civil Environmental Land Building Engineering and Chemistry, DICATECh, Politecnico di Bari, Via Orabona 4, Bari, 70125, Italy

³INFN, Section of Bari, I-70126, Italy

⁴Laboratory for Bioinspired, Bionic, Nano, Meta Materials & Mechanics, University of Trento, Via Mesiano 77, Trento, 38123, Italy

⁵School of Engineering and Materials Science, Queen Mary University of London, Mile End Road, London, E1, U.K.

(*Corresponding author e-mail: stefano.giordano@univ-lille.fr)

(Dated: 1 May 2025)

Mechanically interlocked polymers and molecules exhibit unique topological, physical, and chemical properties, making them highly promising for applications in molecular machines, molecular switches, artificial muscles, nano-actuators, nano-sensors, and biomedical technologies. While significant progress has been made in their synthesis and practical implementation, theoretical studies remain underexplored. In this work, we examine the role of entropic forces in daisy chain structures incorporating rotaxanes, with the ultimate goal of characterizing entropic nano-springs for use in nanomechanics and nanotechnology. Potential applications include artificial cytoskeletons, synthetic cells, and nano-mechanical logic gates.

I. INTRODUCTION

Mechanically interlocked polymers (MIPs) are an extension of mechanically interlocked molecules (MIMs), which are chemical structures incorporating mechanical or topological bonds. MIPs can thus be considered macromolecular versions of MIMs. The inclusion of mechanical bonds imparts significant conformational freedom while preserving the spatial associations between their components.¹⁻⁴

The interesting aspect of these mechanical bonds is that they are not covalent but purely topological, thereby introducing a class of molecules and macromolecules that are entirely original and innovative.⁵ The chemistry of structures that interact non-covalently is known as supramolecular chemistry.^{6,7} In addition to topological bonds, it also includes

hydrogen bonding, hydrophobic and hydrophilic forces, van der Waals forces, and electrostatic effects. These weak non-covalent bonding strategies are central in the growth, synthesis and properties of supramolecular structures.⁸⁻¹⁰

These structures have gained significant attention since Jean-Pierre Sauvage, Sir J. Fraser Stoddart, and Bernard L. Feringa were awarded the Nobel Prize in Chemistry in 2016 for their pioneering work on molecular machines and rotaxanes. A vast number of structures are now available and widely used in nanotechnology.¹¹ For instance, we can mention catenane, rotaxane, and daisy chains.

A catenane is a molecular structure consisting of two or more interlocked rings that are mechanically bonded without covalent connections (see Fig. 1, left panel). The rings are free to move relative to each other, making catenanes and polycatenanes a key component in molecular machines and nanotechnology.^{3,12,13}

A rotaxane is composed of a linear molecular dumbbell thread encircled by a ring, with bulky groups at the ends of the thread to prevent the ring from slipping off (see Fig. 1, right panel). This mechanical bond allows for controlled motion between the thread and the ring, making rotaxanes and polyrotaxanes ideal for applications in molecular electronics and nanomechanics.¹⁴⁻¹⁶ Moreover, bistable rotaxanes, which include two different recognition sites or stations, have attracted considerable attention as molecular switches and machines because of their adjustable geometrical, physical and chemical properties.¹⁷⁻²⁰

Daisy chains are a specific type of mechanically interlocked structure formed by multiple rings or loops connected in a chain-like arrangement through sliding segments (see Fig. 2a). These structures can exhibit sliding or rotational motion, often used in designing responsive materials and arti-

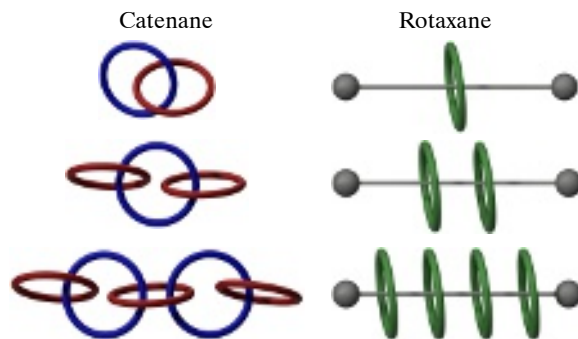


FIG. 1. Catenane, polycatenane, rotaxane, and polyrotaxane structures. The spheres at the ends of rotaxane and polyrotaxane should be larger than the rings to prevent them from slipping out; here, they are shown smaller only for illustrative purposes.

cial muscles (see Fig. 2b).^{2,21–25}

The utility of these supramolecular structures has already been clearly demonstrated for many applications including chemosensors,²⁶ catalysis,²⁷ molecular machines,^{28,29} biomaterials,^{30,31} molecular electronic devices,^{32,33} molecular transporters,³⁴ drug delivery,³⁵ and elastic materials.^{36–38} The synthesis of such supramolecular entities has a considerable impact on their properties and many different techniques were developed throughout the years. Such techniques are often based on the use of templates. These strategies take advantage of the use of affinity sites placed at the different interlocked counterparts, or in their precursors, to finally access the target molecule.¹⁶ More sophisticated techniques allow for more control on the structure construction, like self-assembly techniques,³⁹ molecular pumping techniques,⁴⁰ or thermodynamic control.⁴¹

The ability of these structures to generate force at molecular level has been proved by using the atomic force microscope (AFM).^{42–45} Being able to control the structural properties of rotaxanes and daisy chains open doors to technological advances in areas such as molecular machinery and material science among others. Some studies were recently directed into using rotaxanes as piston motors using the entropy of rings to exert a pressure on a given target.^{46–49} Bistable rotaxanes, in which the dumbbell component contains two different recognition stations for the ring, effectively create two different translational isomers.¹⁷ The transition between these two states operates through oxidation-reduction principles, and nanomechanical actuators have been developed with this scheme.²⁸

In this context, statistical mechanics investigations have been performed to study the conformational isomers of linear rotaxanes,⁵⁰ and the threading of a ring or small tube onto a rod.⁵¹ Other interesting theoretical studies concern the mechanical conformers of particular catenanes,⁵² the fluctuations and switching properties of triangular cyclic rotaxanes,⁵³ and the isotropic-nematic transition in rotaxane liquid crystals.⁵⁴

In contrast to most other polyrotaxanes, which only exhibit rotational and translational degrees of freedom of the rings, daisy chains are particular structures that can alter the length of the polymer, and induce elongation like an elastic material. For this reason, we study in this work the thermoelastic behavior of a particular structure obtained by combining a daisy chain with rotaxane rings. The basic idea is to design entropic nano-springs with applications to nanomechanics. The versatility of the proposed scheme allows tuning both the linear and nonlinear behaviour of such structures. At molecular scale, temperature has a considerable impact and therefore the analysis is conducted through statistical mechanics approaches.⁵⁵

First of all, in Section II, we study the possibility of generating a pressure from a rotaxane ring gas. To this end, we used both the Gibbs statistical ensemble at constant force, and the Helmholtz statistical ensemble at constant extension, and proved the equivalence of the two ensembles in the thermodynamic limit (i.e. for a large number of rotaxane rings).^{56–58}

Then, in Section III, we consider a one-dimensional daisy chain where we introduce, in each segment, two populations of rotaxane rings, to the left and right of the main sliding ring,

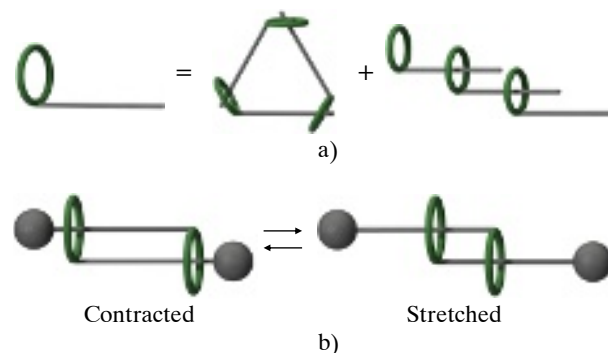


FIG. 2. Daisy chain structures: a) basic element and examples of complex structures; b) sliding structure used as a unit of artificial muscles (contracted and stretched).

see Fig. 4. These two one-dimensional gases have the ability to greatly influence the elastic response of the system, in both linear and nonlinear features.

In the following Section IV, we generalise the previous theory to the case of a three-dimensional daisy chain in which segments can float freely in three dimensions, see Fig. 7. We also show how the freely-jointed chain (FJC) model is a special case of the proposed scheme, composed of a daisy chain with rotaxanes.

In both the one- and three-dimensional cases, we are able to determine the effective elastic constant, the properties in unstressed condition, i.e. without applied external forces, and the overall nonlinear response of the system as a function of the physical and geometric properties of the structure. We also develop asymptotic expressions valid for large values of the applied force. The comparison between one-dimensional and three-dimensional geometry is discussed in depth to explain the important topological differences.

II. THERMODYNAMIC BEHAVIOUR OF A ONE-DIMENSIONAL POLYROTAXANE GAS

In order to grasp how a daisy chain behaves when subjected to a force, we first show the response of a one-dimensional ring-gas polyrotaxane. We consider a polyrotaxane composed of N rings arranged along the x -axis with these two main constraints: (i) the position at $x = 0$ is an ideal wall where the rotaxanes can only be reflected; (ii) one ring cannot pass through another ring and therefore the order of the N rings cannot be changed. In other words, by denoting the positions of the rings as x_1, x_2, \dots, x_N , we can define the following configurational space $\Omega \subset \mathbb{R}^N$ (see Fig. 3)

$$\Omega = \left\{ (x_1, x_2, \dots, x_N) \in \mathbb{R}^N : \begin{cases} 0 < x_1 < x_2 \\ x_1 < x_2 < x_3 \\ \dots \\ x_{N-2} < x_{N-1} < x_N \end{cases} \right\}. \quad (1)$$

In order to study the thermoelastic response of the polyrotaxane system, we can analyze its compression response, which

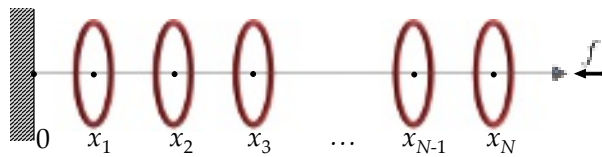


FIG. 3. Illustration of the polyrotaxane gas model where x_1, x_2, \dots, x_N identify the position of each rings along the x -axis. The applied force f is negative to keep the system confined.

is generated by entropic forces alone. We perform this study under two distinctive statistical ensembles corresponding to different boundary conditions: the Gibbs ensemble and the Helmholtz ensemble.

A. The Gibbs statistical ensemble

The Gibbs ensemble, or isotensional ensemble, is characterized by the application of a deterministic force at the end of the system. The overall extension of the system, which is a random variable, is then observed. In our case, a force f is applied on the last ring, characterized by its position x_N . Therefore, the total potential energy is $V(x_1, \dots, x_N) = -fx_N$ as there are no other forces applied to the system. Of course, this force will always be negative ($f < 0$, see Fig. 3) to keep the system confined, as is also seen in the following calculations and discussions.

It is important now to better justify and discuss these assumptions, already adopted in other works.^{46–49} Indeed, regarding the interactions between the rings and between each ring and the main chain, one might think of adding other forms of conservative and dissipative interactions.

As for conservative interactions, they would be described by an interaction potential energy, which determines the forces transmitted between links or with the main chain. These effects are neglected here because they are assumed to be at a very short range. Thus, they only intervene when two links are close to colliding. The fact that the rings collide with no possibility of passing through other rings is quite realistic (for reasonable temperatures) since they all have the same size and a rather complex molecular structure that increases their thickness and rigidity. Collisions in this work are therefore considered ideal and thus described by a potential energy consisting of a wall with infinite energy. The total interaction energy is then taken to be zero except at the collision points: the collision situation is, however, taken into account geometrically and automatically through the precise description of the integration domain in the partition functions.

As for dissipative phenomena, particularly the possible friction between rings and the main chain, they are not described and used in this work, but may actually be present. The reason we can neglect these dissipative phenomena lies in the fact that we are working at thermodynamic equilibrium, and friction affects only the relaxation regime toward equilibrium and not the equilibrium itself. In fact, we know from Langevin's model or similar models that relaxation toward equilibrium

in a given system is described by the combination of thermal fluctuations (noise) and dissipation (with a well-defined fluctuation-dissipation relation $D = K_B T \beta$, where D is the diffusion constant, T is the temperature and β is the friction coefficient). The effect of friction, in this scheme, is to change the relaxation time $\tau \sim 1/\beta$ (which decreases as the coefficient of friction increases), both at the classical and quantum level.^{59–61} In other words, one could say that the system is viscoelastic with a small viscosity, and that we focus here on its elastic component.

We also assumed that the main segments remain straight during the evolution of the system. In reality, there can evidently be flexures of these segments that should not, however, affect the behavior of the system, particularly when their length is not much larger than the characteristic persistence length of the adopted molecules (for reasonable temperatures).⁵⁷

All these effects may play a role in the system, but they are typically secondary compared to the interlocking and entropic effects considered in this work. Possible extensions can, of course, be explored in future studies

Based on these premises, the Gibbs partition function for the system in Fig. 3 can be written as

$$Z_g(f) = \int_{\Omega \subset \mathbb{R}^N} \exp\left(\frac{fx_N}{k_B T}\right) dx_1 \dots dx_N. \quad (2)$$

To perform the integration, we adopt the change of variables

$$\begin{cases} \xi_1 = x_1 > 0, \\ \xi_2 = x_2 - x_1 > 0, \\ \dots \\ \xi_N = x_N - x_{N-1} > 0, \end{cases} \quad (3)$$

from which we deduce that $x_N = \sum_{i=1}^N \xi_i$. Since the Jacobian determinant of the transformation is unitary, the partition function becomes

$$\begin{aligned} Z_g(f) &= \int_{\{\xi_i \geq 0 \forall i=1, \dots, N\}} \exp\left(\frac{f \sum_{i=1}^N \xi_i}{k_B T}\right) d\xi_1 \dots d\xi_N \\ &= \left[\int_0^{+\infty} \exp\left(\frac{f\xi}{k_B T}\right) d\xi \right]^N = \left(-\frac{k_B T}{f}\right)^N. \end{aligned} \quad (4)$$

As the system remains confined only if the applied force is compressive (in the direction opposite to x -axis), the Gibbs partition function is convergent only if $f < 0$. We remind that the polyrotaxane system acts as a gas and accordingly it generates a pressure that tends to make it expand, which is balanced by the force $f < 0$. Using the classical thermodynamics,^{56–58} we can determine the average position $\langle x_N \rangle$ of the last ring as follows

$$\begin{aligned} \langle x_N \rangle &= k_B T \frac{\partial}{\partial f} \log Z_g = k_B T \frac{\partial}{\partial f} \left[\log \left(-\frac{k_B T}{f} \right)^N \right] \\ &= -\frac{N k_B T}{f}. \end{aligned} \quad (5)$$

Consequently, the applied force and the position of the last ring are linked by the relation

$$\langle x_N \rangle f = -Nk_B T. \quad (6)$$

By replacing f with the “pressure” $-p$, we can find the equation of state for the ring gas within the Gibbs ensemble as $p \langle x_N \rangle = Nk_B T$, which is analogous to the ideal gas law in thermodynamics.

B. The Helmholtz statistical ensemble

In contrast to the isotensional ensemble, the Helmholtz or isometric statistical ensemble imposes a fixed end position rather than a fixed force. In this case, the last ring is supposed to be fixed at x_N . Then, since x_N is no longer a statistical variable, the configurational space $\tilde{\Omega}$ can be redefined as the following subset of \mathbb{R}^{N-1}

$$\tilde{\Omega} = \left\{ (x_1, x_2, \dots, x_{N-1}) \in \mathbb{R}^{N-1} : \begin{cases} 0 < x_1 < x_2 \\ x_1 < x_2 < x_3 \\ \dots \\ x_{N-2} < x_{N-1} < x_N \end{cases} \right\}, \quad (7)$$

where x_N is fixed. Since the potential energy is zero, the partition function has the following form

$$Z_h(x_N) = \int_{\tilde{\Omega} \subset \mathbb{R}^{N-1}} dx_1 \dots dx_{N-1}. \quad (8)$$

We adopt the change of variables

$$\begin{cases} \xi_1 = x_1 > 0, \\ \xi_2 = x_2 - x_1 > 0, \\ \dots \\ \xi_{N-1} = x_{N-1} - x_{N-2} > 0, \end{cases} \quad (9)$$

and we get

$$x_{N-1} = \sum_{i=1}^{N-1} \xi_i \leq x_N. \quad (10)$$

After the application of this change of variables, we can define the new integration domain Ψ , defined below, which is described by a $(N-1)$ -simplex

$$\Psi(x_N) = \{ \xi_i \geq 0 \forall i = 1, \dots, N-1, \sum_{i=1}^{N-1} \xi_i \leq x_N \} \subset \mathbb{R}^{N-1}, \quad (11)$$

and therefore we can rewrite the Helmholtz partition function as

$$Z_h(x_N) = \int_{\Psi(x_N) \subset \mathbb{R}^{N-1}} d\xi_1 \dots d\xi_{N-1}. \quad (12)$$

To calculate the measure of domains obtained from a n -dimensional simplex of height h , referred to as $\sigma(h) \subset \mathbb{R}^n$,

$$\sigma(h) = \{ X_i \geq 0, \forall i = 1, \dots, n, \sum_{i=1}^n X_i \leq h \}, \quad (13)$$

we can use the following formula⁶²

$$\int_{\sigma(h)} dX_1 \dots dX_n = \frac{h^n}{n!} \mathbf{1}(h), \quad (14)$$

where $\mathbf{1}(x)$ is the Heaviside step function, defined as $\mathbf{1}(x)=1$ if $x \geq 0$, and $\mathbf{1}(x)=0$ if $x < 0$. By using this result in Eq. (12), we obtain the expression of the Helmholtz partition function

$$Z_h(x_N) = \frac{x_N^{N-1}}{(N-1)!} \mathbf{1}(x_N). \quad (15)$$

In Eqs. (14) and (15), we included the step functions to emphasize the fact that the expressions found are valid only for $h > 0$ and for $x_N > 0$, respectively. This notation will be especially useful in the next logical steps, where we introduce a relationship between the Gibbs and Helmholtz partition functions.

The average force necessary to impose the Helmholtz condition can be calculated, for $x_N > 0$, as follows⁵⁶⁻⁵⁸

$$\begin{aligned} \langle f \rangle &= -k_B T \frac{\partial}{\partial x_N} \log Z_h = k_B T \frac{\partial}{\partial x_N} \frac{x_N^{N-1}}{(N-1)!} \\ &= k_B T \frac{\partial}{\partial x_N} [\log(x_N^{N-1})] = -\frac{(N-1)k_B T}{x_N}. \end{aligned} \quad (16)$$

The resulting force-extension relation is then obtained in the form

$$\langle f \rangle_{x_N} = -(N-1)k_B T, \quad (17)$$

and by introducing the quantity $p = -f$, we find the gas law under isometric condition as $\langle x_N \rangle p = (N-1)k_B T$. We note that for large values of N , the Helmholtz law given in Eq. (17), and the Gibbs law obtained in Eq. (6) are asymptotically coinciding, which means that the two statistical ensembles are equivalent in the thermodynamic limit. However, one should remember that the statistical variables are different for the two models: while the Gibbs law considers an imposed force f and a corresponding average value of the last position $\langle x_N \rangle$, we have the dual case with $\langle f \rangle$ and x_N in the Helmholtz ensemble. The equivalence of statistical ensembles is a widely studied and debated topic in statistical mechanics,^{56-58,63-68} and there are explicit examples where this equivalence is not respected.⁶⁹⁻⁷³ In addition, the gas model is useful for comparing the thermodynamic limit with the continuum limit in statistical mechanics⁷⁴. Moreover, it is crucial to notice that in both ensembles, the force is purely entropic and therefore temperature-dependent (if the temperature is zero, the force is zero as well). Furthermore, by drawing a comparison between Eq. (2) and Eq. (8), it is possible to discern a connection between the Gibbs and Helmholtz partition functions, which are indeed related through the classical Laplace transform

$$Z_g(f) = \int_{-\infty}^{+\infty} Z_h(x) \exp\left(\frac{fx}{k_B T}\right) dx. \quad (18)$$

Performing the calculation, we obtain

$$\begin{aligned} Z_g(f) &= \int_{-\infty}^{+\infty} \mathbf{1}(x) \frac{x_N^{N-1}}{(N-1)!} \exp\left(\frac{fx}{k_B T}\right) dx \\ &= \frac{1}{(N-1)!} \left(-\frac{f}{k_B T}\right)^{-N} \Gamma(N) = \left(-\frac{k_B T}{f}\right)^N, \end{aligned} \quad (19)$$

with the condition $f < 0$, where $\Gamma(z) = \int_0^{+\infty} e^{-t} t^{z-1} dt$ is the Gamma function, and $\mathbf{1}(x)$ is the Heaviside function previously defined. The result in Eq. (19) exactly corresponds to Eq. (4), confirming the validity of this approach. The Laplace relation between the partition functions is very important because it is always valid regardless of the equivalence of the ensembles in the thermodynamic limit. When the thermodynamic limit is verified, the relationship is simplified and reduces to the Legendre transform between the corresponding free energies $\mathcal{G} = -k_B T \log Z_g$, and $\mathcal{F} = -k_B T \log Z_h$.^{56,57,63}

We have shown that a set of rotaxane rings inserted in a linear chain is able to exert an entropic force dependent on the total number of elements. We exploit in the sequel this result to study more complex structures that can be used to design entropic nano-springs.

III. ONE-DIMENSIONAL DAISY CHAIN WITH ADDITIONAL RINGS

While we have developed a thermodynamic model for a single polyrotaxane system in Section II, daisy chains present more complex structures and therefore need further study in order to determine their thermoelastic response. Here, we use the results from Section II to determine the force-extension law for a one-dimensional daisy chain with additional rotaxane rings.

A. Force-extension law of a 1D daisy chain

We consider a daisy chain aligned along the x -axis with additional rings within the Gibbs ensemble (under isotensional condition). This system is made of N segments, each of length ℓ , as depicted in Fig. 4. Each segment contains two different populations of rotaxane rings, separated by the main rings (a), (b), (c), and so on. More specifically, there are n rotaxane rings on the left, and m on the right of each main sliding ring. The position of the main rings (in green in Fig. 4) are identified by the abscissae x^J , where $1 \leq J \leq N$. The geometry of the left population of rotaxane rings is described by the variable y_i^J , where $1 \leq i \leq n$ and $1 \leq J \leq N$, each representing the distance between the adjacent rotaxanes j and $j-1$; similarly, the right population rings is described by the distances z_i^J , with $1 \leq i \leq m$ and $1 \leq J \leq N$. We remark that the subscript i refers to rotaxane rings (both on the left and on the right of each main sliding ring), and the superscript J denotes the J -th segment of the daisy chain. Moreover, the first segment's left-end is fixed at the origin, while the last segment's right-end is subjected to an applied force f (as is typically done in force spectroscopy experiments). Finally, as in the case of the one-dimensional polyrotaxane gas, each ring cannot pass through another adjacent ring (including the sliding main rings), and it cannot leave the segment of length ℓ . All the main rings (in green) are subject to the same restrictions and constraints as the other freely moving rings (already discussed for the gas model).

Under these premises, we can write the Gibbs partition function for the overall system in the form

$$Z_g(f) = \int_0^\ell \int_0^\ell \cdots \int_0^\ell \left[\exp\left(\frac{f \sum_{J=1}^N x^J}{k_B T}\right) \times \prod_{J=1}^N \int_{\Delta_J} dy_1^J dy_2^J \cdots dy_n^J \times \prod_{J=1}^N \int_{\Theta_J} dz_1^J dz_2^J \cdots dz_m^J \right] dx^1 dx^2 \cdots dx^N, \quad (20)$$

where the two internal integrals are evaluated, respectively, over domains $\Delta_J \subset \mathbb{R}^n$ and $\Theta_J \subset \mathbb{R}^m$, defined as

$$\Delta_J = \{y_i^J \geq 0, \forall 1 \leq i \leq n, \sum_{i=1}^n y_i^J \leq x^J\}, \quad \forall 1 \leq J \leq N, \quad (21)$$

concerning the rotaxane populations on the left of the main rings, and

$$\Theta_J = \{z_i^J \geq 0, \forall 1 \leq i \leq m, \sum_{i=1}^m z_i^J \leq \ell - x^J\}, \quad \forall 1 \leq J \leq N, \quad (22)$$

describing the behavior of the rotaxane populations on the right of the main rings. These internal integrals must be considered to take into account the effects of the rings located in the left and right regions of each daisy chain segment. We know that the partition function must sum over all possible configurations of the system, taking into account all its subsystems. This is done by integrating the Boltzmann factor, calculated with the total energy of the system, over all the variables that define its microscopic state. Since all the rings of each one-dimensional gas (to the left and right of each main ring) are confined to a region of extent x^J (for populations placed to the left) and to a region of extent $\ell - x^J$ (for populations placed to the right), and since all x^J variables must be integrated in the partition function, it follows that the integrals over the populations of free rings must be contained in the integrals over the x^J coordinates, defining the positions of the main rings. Such positioning of the integrals ensures that the partition function no longer depends on the internal configurational variables but only on the external force, and temperature of the system. This example shows how the structural constraints that define the configuration of the system can alter its thermodynamic properties and, in particular, its entropy (and relative entropic forces) through the mathematical form that the partition function takes. Moreover, the exponential term in Eq. (20) corresponds to the contribution of all the sliding segments and of the force f applied to the last element of the chain. That said, Eq. (20) can be simplified by means of Eq. (14) and we get

$$Z_g(f) = \int_0^\ell \int_0^\ell \cdots \int_0^\ell \left[\exp\left(\frac{f \sum_{J=1}^N x^J}{k_B T}\right) \times \prod_{J=1}^N \frac{(x^J)^n}{n!} \times \prod_{J=1}^N \frac{(\ell - x^J)^m}{m!} \right] dx^1 dx^2 \cdots dx^N. \quad (23)$$

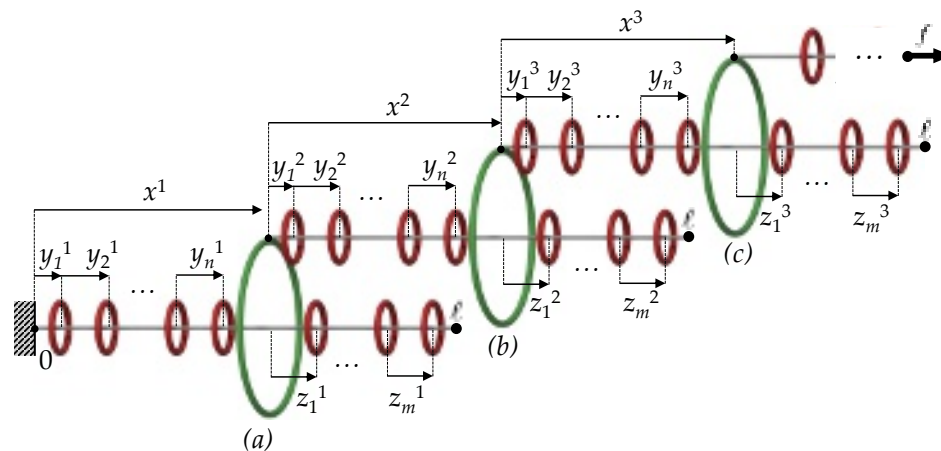


FIG. 4. Illustration of the model for the one-dimensional daisy chain made of N segments of length ℓ . In the J -th segment, x^J identifies the position of the main rings (a), (b), (c), and so on (in green). Each main ring separates two different populations of rotaxanes (in red): on the left, there are n rotaxanes, with the distances between the adjacent rings j and $j-1$ identified by the quantity y_j^J , where $1 \leq i \leq n$ and $1 \leq J \leq N$; on the right there are m rotaxanes, where, analogously to the case of the left population, the distances between adjacent rings are described by z_i^J , with $1 \leq i \leq m$ and $1 \leq J \leq N$. No ring can exchange position with an adjacent ring (including with main rings in green), and no ring can leave the segment of length ℓ (the green rings are larger only for representational necessity).

It is now easily seen that the remaining N integrals can be factorized as follows

$$\begin{aligned} Z_g(f) &= \int_0^\ell \frac{(x^1)^n (\ell - x^1)^m}{n!m!} \exp\left(\frac{fx^1}{k_B T}\right) dx^1 \\ &\times \dots \times \int_0^\ell \frac{(x^N)^n (\ell - x^N)^m}{n!m!} \exp\left(\frac{fx^N}{k_B T}\right) dx^N \\ &= \frac{1}{(n!m!)^N} \left[\int_0^\ell x^n (\ell - x)^m \exp\left(\frac{fx}{k_B T}\right) dx \right]^N. \end{aligned} \quad (24)$$

We have obtained a simplified form for the Gibbs partition function for a one-dimensional daisy chain. By further changing the variable of the integral through the transformation $t = x/\ell$, the Gibbs partition function assumes the new form

$$Z_g(f) = \left[\int_0^1 \frac{(t\ell)^n (\ell - t\ell)^m}{n!m!} \exp\left(\frac{ft\ell}{k_B T}\right) \ell dt \right]^N, \quad (25)$$

or, equivalently

$$Z_g(\eta) = C \left[\int_0^1 t^n (1-t)^m \exp(\eta t) dt \right]^N, \quad (26)$$

where $\eta = f\ell/(k_B T)$ is the non-dimensional or normalized applied force, and $C = \left[\frac{\ell^{n+m+1}}{n!m!} \right]^N$ is a non-influential constant. The knowledge of the partition function makes it possible to calculate all kinds of average values and thus to study the thermodynamics of the system. In particular, we can determine the force-extension relation by calculating the average value of the total extension $\bar{x} = \sum_{J=1}^N x^J$. We use the classical thermodynamic relations,^{56,57} which lead to

$$\begin{aligned} \langle \bar{x} \rangle &= k_B T \frac{\partial \log Z_g(f)}{\partial f} = \ell \frac{\partial \log Z_g(\eta)}{\partial \eta} \\ &= N\ell \frac{\int_0^1 t^{n+1} (1-t)^m e^{\eta t} dt}{\int_0^1 t^n (1-t)^m e^{\eta t} dt}. \end{aligned} \quad (27)$$

First of all, we can analyze the equilibrium position of the chain without any applied force. By imposing $f = 0$ (i.e. $\eta = 0$), the equilibrium point of the system can be calculated as

$$\langle \bar{x} \rangle \Big|_{\eta=0} = N\ell \frac{\int_0^1 t^{n+1} (1-t)^m dt}{\int_0^1 t^n (1-t)^m dt}. \quad (28)$$

We can now use the Gamma function $\Gamma(\mu) = \int_0^{+\infty} e^{-\tau} \tau^{\mu-1} d\tau$, and the Beta function $B(\alpha, \beta) = \int_0^1 \tau^{\alpha-1} (1-\tau)^{\beta-1} d\tau$, satisfying the properties $\Gamma(n) = (n-1)!$, $B(\alpha, \beta) = B(\beta, \alpha)$, and $B(\alpha, \beta) = \Gamma(\alpha)\Gamma(\beta)/\Gamma(\alpha+\beta)$.^{75,76} From these properties it is possible to deduce the equilibrium extension of the chain in the following form

$$\begin{aligned} \langle \bar{x} \rangle \Big|_{\eta=0} &= N\ell \frac{B(n+2, m+1)}{B(n+1, m+1)} \\ &= N\ell \frac{\Gamma(n+2)\Gamma(m+1)}{\Gamma(n+m+3)} \frac{\Gamma(n+m+2)}{\Gamma(n+1)\Gamma(m+1)} \\ &= N\ell \frac{(n+1)!m!}{(n+m+2)!} \frac{(n+m+1)!}{n!m!} \\ &= N\ell \frac{n+1}{n+m+2}. \end{aligned} \quad (29)$$

This obviously implies that the average extension of the sliding segments are given by

$$\langle x^1 \rangle \Big|_{\eta=0} = \langle x^2 \rangle \Big|_{\eta=0} = \dots = \langle x^N \rangle \Big|_{\eta=0} = \ell \frac{n+1}{n+m+2}. \quad (30)$$

This result contains interesting information, as it links the properties of rotaxane populations with the equilibrium positions of the sliding segments. Three relevant cases can be

mentioned

$$\begin{cases} \langle x^J \rangle_{\eta=0} = \frac{\ell}{2} & \text{if } n = m, \\ \langle x^J \rangle_{\eta=0} \rightarrow 0 & \text{if } m \rightarrow +\infty, \\ \langle x^J \rangle_{\eta=0} \rightarrow \ell & \text{if } n \rightarrow +\infty. \end{cases} \quad (31)$$

Of course, when the number of rings is equal at the left and right of the separating element, the two pressures balance and we obtain the central position at equilibrium. We observe that the second and third cases represent the situations of high density of right ring gas, and high density of left ring gas, respectively. When m tends to infinity, the gas on the right becomes dominant, and the main ring shifts to the left, ultimately reaching the extreme position 0. Similarly, when n tends to infinity, the gas on the left becomes dominant, and the main ring shifts to the right, reaching the extreme position ℓ . From Eq. (27), it is possible to plot the force-extension curve $\frac{\langle \tilde{x} \rangle}{N\ell}$ versus η (see Fig. 5) either by numerical integration or using its closed form expression (demonstrated in Appendix A)

$$\langle \tilde{x} \rangle = -N\ell \frac{\sum_{h=0}^m \binom{m}{h} \frac{(n+1+h)!}{\eta^{h+1}} \left[e^{\eta} \sum_{k=0}^{n+h+1} \frac{(-\eta)^k}{k!} - 1 \right]}{\sum_{h=0}^m \binom{m}{h} \frac{(n+h)!}{\eta^h} \left[e^{\eta} \sum_{k=0}^{n+h} \frac{(-\eta)^k}{k!} - 1 \right]}. \quad (32)$$

This relation describes the fully nonlinear thermomechanical behavior of the system. In addition to being helpful for plotting the force-extension curve (see Fig. 5), this expression can also be used to determine the two following asymptotic behaviours

$$\begin{aligned} \eta \rightarrow +\infty &\implies \langle \tilde{x} \rangle \sim N\ell \left(1 - \frac{m+1}{\eta} \right), \\ \eta \rightarrow -\infty &\implies \langle \tilde{x} \rangle \sim -N\ell \left(\frac{n+1}{\eta} \right). \end{aligned} \quad (33)$$

For illustrative purposes, in Fig. 5, both asymptotes, as well as the tangent at the equilibrium position $\eta = 0$, are represented for $n = m = 1$. Note that in Fig. 5, and all the following ones, there are no specified units for the quantities on the abscissa and ordinate axes: this corresponds to the fact that these quantities are always dimensionless as they are normalized. Note also that in Fig. 5 and subsequent figures we have always represented the normalized extension but one could also represent the strain (or stretch) defined as $\varepsilon = \left(\langle \tilde{x} \rangle - \langle \tilde{x} \rangle_{\eta=0} \right) / \langle \tilde{x} \rangle_{\eta=0}$.

Other examples of the application of Eq. (32) can be found in Fig. 6, where we have plotted the nonlinear response for different populations described by the parameters n and m . In the top panel we have fixed $m = 1$ and varied n . It can be seen how the nonlinear response varies as n varies, and how the point of equilibrium moves upward following the increasing law $\frac{\langle \tilde{x} \rangle}{N\ell} = \frac{n+1}{n+m+2} = \frac{n+1}{n+3}$. In the central panel we have variable values of $n = m$. In this case we see how the system becomes more rigid as $n = m$ increases, while the equilibrium point remains fixed at $\frac{\langle \tilde{x} \rangle}{N\ell} = \frac{n+1}{n+m+2} = \frac{1}{2}$, when the applied force is

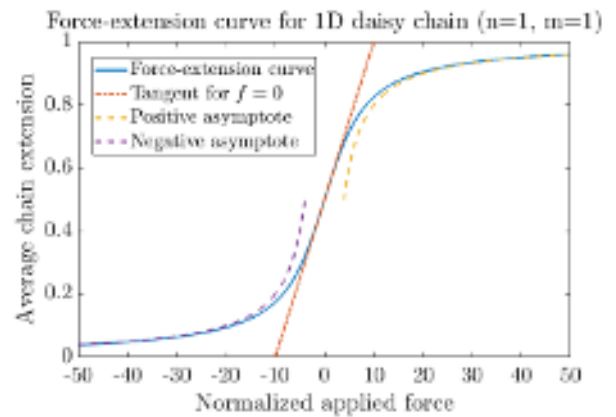


FIG. 5. Force-extension curve representing $\frac{\langle \tilde{x} \rangle}{N\ell}$ versus η for a one-dimensional daisy chain. We adopted the parameters $n = 1$ and $m = 1$. We plotted the asymptotes for very large positive and negative force, and the tangent for $f = 0$, which has a slope of $\frac{1}{20}$, see Eq. (34).

zero. Finally, in the bottom panel we have fixed $n = 1$ and varied m . It can be seen how the nonlinear response varies as m varies, and how the point of equilibrium moves downward following the decreasing law $\frac{\langle \tilde{x} \rangle}{N\ell} = \frac{n+1}{n+m+2} = \frac{2}{m+3}$, when the applied force is zero.

B. Effective elastic constant of the one-dimensional daisy chain

Daisy chains with rotaxane rings show great potential in material science as nanoscopic entropic springs. For that reason, identifying the effective elastic constant is important to better understand the behavior of these macromolecules. The elastic constant K_{eff} can be obtained by calculating the slope of the force-extension curve at the equilibrium point, i.e. $1/K_{\text{eff}} = \left. \frac{\partial \langle \tilde{x} \rangle}{\partial f} \right|_{f=0}$. The corresponding calculation can be found in Appendix B, and the final result is

$$K_{\text{eff}} = \frac{k_B T (n+m+2)^2 (n+m+3)}{N\ell^2 (n+1)(m+1)}. \quad (34)$$

This formula gives the effective elastic stiffness as a function of the temperature T , the segment length ℓ , the number of segments N , and the rotaxanes numbers m and n . Naturally, the overall behavior is nonlinear, and this parameter thus represents the elastic response under small applied forces. We remark that the expression is symmetric in the parameters n and m , as expected for this one-dimensional case. As a side note, it is interesting to calculate the elastic coefficient when $n = m$. In this case, $\langle \tilde{x} \rangle(0) = N\ell/2$, and the effective elastic coefficient becomes

$$K_{\text{eff}} = \frac{4k_B T}{N\ell^2} (2n+3). \quad (35)$$

For large values of n , we have the asymptotic behaviour

$$K_{\text{eff}} \underset{n \rightarrow \infty}{\sim} 8 \frac{nk_B T}{N\ell^2}, \quad \text{or equivalently} \quad \frac{K_{\text{eff}} \ell^2}{2k_B T} \underset{n \rightarrow \infty}{\sim} 4 \frac{n}{N}, \quad (36)$$

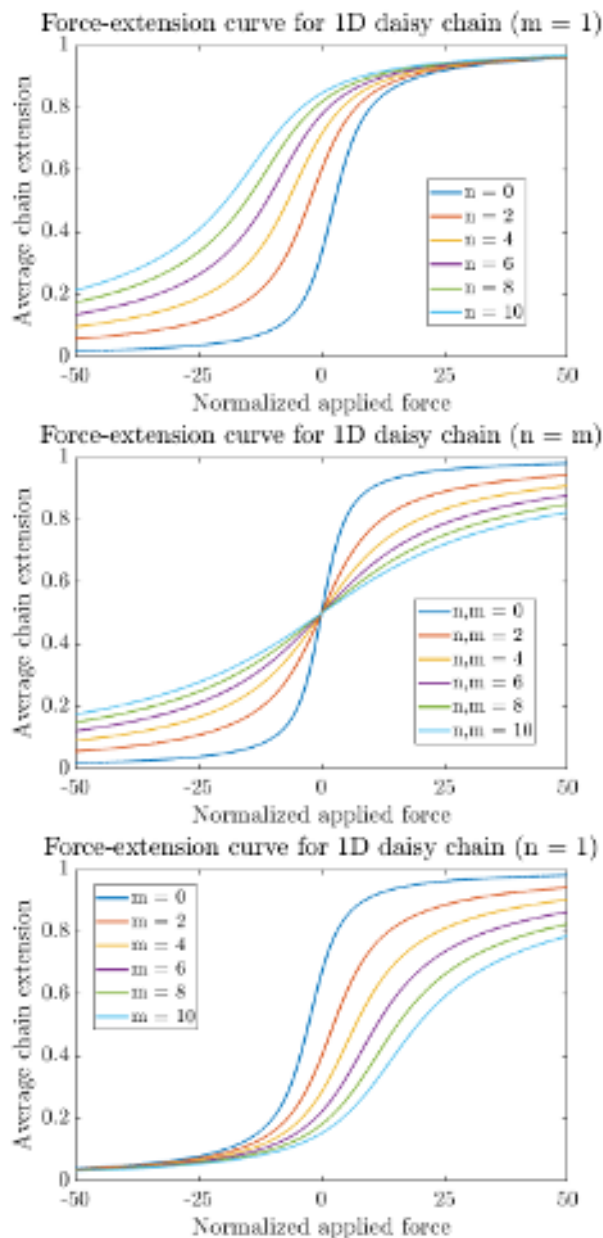


FIG. 6. Extension-force curves representing $\langle \tilde{x} \rangle / N\ell$ versus η for a one-dimensional daisy chain: in top panel, the number n of rotaxanes to the left of the main ring varies from 0 to 10, while the number of rotaxanes to the right of the main ring is $m = 1$. For $f = 0$, we have that $\langle \tilde{x} \rangle / N\ell = \frac{n+1}{n+m+2} = \frac{n+1}{n+3}$, increasing with n . In the central panel, we have $n = m$, varying from 0 to 10. For $f = 0$, we have that $\langle \tilde{x} \rangle / N\ell = \frac{n+1}{n+m+2} = \frac{1}{2}$. Finally, in the bottom panel, the number m of rotaxanes to the right of the main ring varies from 0 to 10, while the number of rotaxanes to the left of the main ring is $n = 1$. For $f = 0$, we have that $\langle \tilde{x} \rangle / N\ell = \frac{n+1}{n+m+2} = \frac{2}{m+3}$, decreasing with m .

which shows that the elastic to thermal energy ratio is given by $4n/N$. Thus for $n = m$, and large values of n , the elastic constant is proportional to n .

We finally observe that Eq. (34) can be used to explain the effective elastic constant of the systems studied in Fig. 6. The

top panel is described by the relation $K_{\text{eff}} = \frac{k_B T}{2N\ell^2} \frac{(n+3)^2(n+4)}{n+1}$, the central panel by Eq. (35), and the bottom panel by the relation $K_{\text{eff}} = \frac{k_B T}{2N\ell^2} \frac{(m+3)^2(m+4)}{m+1}$. In each case, the effective elastic constant is always increasing as the rotaxane populations increase, both to the left and right of the main ring.

C. Extension to heterogeneous segments

While in the previous study, every segment was considered to have the same population of rotaxanes on the left (n elements) and on the right (m elements) of the main separating ring, the results for homogeneous daisy chains can easily be generalized to the case with heterogeneous values of the parameters. In this case, for each J -th sliding segment, the left and right rotaxane populations assume respectively the values n_J and m_J . By using Eq. (24), we see that the partition function can be factorized and assumes the new form

$$Z_g(f) = \prod_{J=0}^N \int_0^\ell \frac{(x^J)^{n_J} (\ell - x^J)^{m_J}}{(n_J)!(m_J)!} \exp\left(\frac{fx^J}{k_B T}\right) dx^J. \quad (37)$$

Moreover, the average extension of the chain can be determined by means of the following generalization

$$\langle \tilde{x} \rangle = \ell \sum_{J=1}^N \frac{\int_0^1 t^{n_J+1} (1-t)^{m_J} e^{\eta t} dt}{\int_0^1 t^{n_J} (1-t)^{m_J} e^{\eta t} dt}. \quad (38)$$

The equilibrium extension, obtained for $f = 0$, is given by the expression

$$\langle \tilde{x} \rangle(0) = \ell \sum_{J=1}^N \frac{n_J + 1}{n_J + m_J + 2}, \quad (39)$$

and finally, the effective elastic coefficient is obtained as

$$K_{\text{eff}} = \frac{k_B T}{\ell^2} \frac{1}{\sum_{J=1}^N \frac{(n_J+1)(m_J+1)}{(n_J+m_J+2)^2(n_J+m_J+3)}}. \quad (40)$$

These generalized expressions can be used to finely tailor the elastic response of the system, including the linear effective elastic constant and the nonlinear behavior.

We want to emphasize that in the previous calculations we have considered for the daisy chain system only the Gibbs ensemble, at fixed force, for two different reasons: first, it is sufficient to explain the elastic properties of the system; second, if we consider the Helmholtz ensemble, at fixed extension, the calculations cannot be developed in closed form and thus the possibility of easily interpreting the results is lost. All this also applies to the next Section.

IV. THREE-DIMENSIONAL DAISY CHAIN WITH ADDITIONAL RINGS

We assume now that the chain can fluctuate in the three-dimensional space and is no longer constrained to move along a fixed direction. We first study a simple three-dimensional

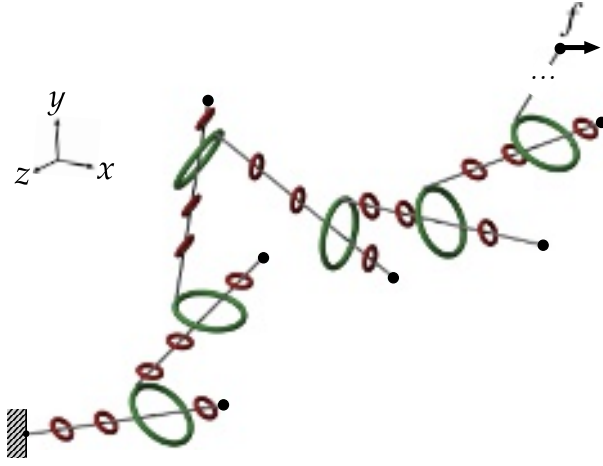


FIG. 7. Illustration of the geometry of a three-dimensional daisy chain with additional rings (in red). As an example, we considered the case with $n = 2$ and $m = 1$. As before, no ring can exchange position with an adjacent ring (including with main rings in green), and no ring can leave the segment of length ℓ (the green rings are larger only for representational necessity).

chain of interacting points through (nearest neighborhood) conservative central forces depending on the points distance. An external force is acting only on last material point. We introduce here an arbitrary potential energy, and then we apply this system to the study of daisy chains with additional rings (rotaxanes), as represented in Fig. 7.

A. Partition function for a chain of interacting material points

We start by introducing the analysis of an arbitrary three-dimensional chain of material points. This chain is composed of N points interacting through a pairwise potential energy and subject to an external force. Thus, the system will be analyzed in the Gibbs isotensional ensemble. Hence, the total energy reads

$$U_T(\vec{r}_1, \dots, \vec{r}_N) = \sum_{i=1}^N U(\|\vec{r}_i - \vec{r}_{i-1}\|) - \vec{f} \cdot \vec{r}_N, \quad (41)$$

where $\vec{r}_1, \dots, \vec{r}_N$ are the position vectors identifying the points, $U(\xi)$ is the potential energy between two adjacent points at distance ξ , and \vec{f} is the force applied to the last point of the chain. We considered $\vec{r}_0 = 0$ (the point where the chain is tethered). The Gibbs partition function of the system can be written as

$$\begin{aligned} Z_g(\vec{f}) &= \int_{\mathbb{R}^{3N}} \exp \left[-\sum_{i=1}^N \frac{U(\|\vec{r}_i - \vec{r}_{i-1}\|)}{k_B T} + \frac{\vec{f} \cdot \vec{r}_N}{k_B T} \right] d\vec{r}_1 \dots d\vec{r}_N \\ &= \int_{\mathbb{R}^{3N}} \prod_{i=1}^N \exp \left[-\frac{U(\|\vec{r}_i - \vec{r}_{i-1}\|)}{k_B T} \right] \exp \left[\frac{\vec{f} \cdot \vec{r}_N}{k_B T} \right] d\vec{r}_1 \dots d\vec{r}_N \end{aligned} \quad (42)$$

Let us define the bond vectors $\vec{\xi}_1 = \vec{r}_1 - \vec{r}_0, \dots, \vec{\xi}_N = \vec{r}_N - \vec{r}_{N-1}$, so that $\vec{r}_N = \sum_{i=1}^N \vec{\xi}_i$. We get

$$\begin{aligned} Z_g(\vec{f}) &= \int_{\mathbb{R}^3} \dots \int_{\mathbb{R}^3} \prod_{i=1}^N \exp \left[-\frac{U(\|\vec{\xi}_i\|)}{k_B T} + \frac{\vec{f} \cdot \vec{\xi}_i}{k_B T} \right] d\vec{\xi}_1 \dots d\vec{\xi}_N \\ &= \left(\int_{\mathbb{R}^3} \exp \left[-\frac{U(\|\vec{\xi}\|)}{k_B T} + \frac{\vec{f} \cdot \vec{\xi}}{k_B T} \right] d\vec{\xi} \right)^N. \end{aligned} \quad (43)$$

Again, we obtain the partition function as a power of a quantity describing a single element, since all elements are statistically independent on each other. We note that the system is fully isotropic and therefore we can consider any direction for the applied force \vec{f} . To simplify the analysis, we fix $\vec{f} = (0, 0, f)$, and we adopt spherical coordinates for the vector $\vec{\xi}$. It means that $d\vec{\xi} = \xi^2 \sin \theta d\theta d\phi d\xi$, $\|\vec{\xi}\| = \xi$, and $\vec{f} \cdot \vec{\xi} = f\xi \cos \theta$. The partition function can be then simplified in the form

$$\begin{aligned} Z_g(f) &= \left\{ \int_0^{+\infty} \int_0^{2\pi} \int_0^\pi \exp \left[-\frac{U(\xi)}{k_B T} \right] \right. \\ &\quad \times \exp \left(\frac{f\xi \cos \theta}{k_B T} \right) \xi^2 \sin \theta d\theta d\phi d\xi \left. \right\}^N \\ &= \left\{ 2\pi \int_0^{+\infty} \exp \left[-\frac{U(\xi)}{k_B T} \right] \right. \\ &\quad \times \left[\int_0^\pi \exp \left(\frac{f\xi \cos \theta}{k_B T} \right) \sin \theta d\theta \right] \xi^2 d\xi \left. \right\}^N, \end{aligned} \quad (44)$$

where the inner integral can be solved as

$$\int_0^\pi \exp \left(\frac{f\xi \cos \theta}{k_B T} \right) \sin \theta d\theta = 2 \frac{k_B T}{f\xi} \sinh \left(\frac{f\xi}{k_B T} \right). \quad (45)$$

Finally, we obtain

$$Z_g(f) = C^N \left[\int_0^{+\infty} \exp \left[-\frac{U(\xi)}{k_B T} \right] \frac{\xi}{f} \sinh \left(\frac{f\xi}{k_B T} \right) d\xi \right]^N, \quad (46)$$

where $C = 4\pi k_B T$ is a constant.

The result in Eq. (46) represents the Gibbs partition function for a chain where each couple of adjacent points interact by an arbitrary potential energy U . The determination of the three-dimensional daisy chain partition function relies on this result, which can be helpful for other applications as well. For instance, it can be applied to the freely-jointed chain (FJC) model,⁵⁶ that will be re-obtained later as a daisy chain in specific configurations. Indeed, if the interaction between the material points is purely harmonic, described by $U(\xi) = \frac{1}{2}K(\xi - \ell)^2$, the partition function becomes

$$Z_g(f) = C^N \left[\int_0^{+\infty} e^{-\frac{K}{2k_B T}(\xi - \ell)^2} \frac{\xi}{f} \sinh \left(\frac{f\xi}{k_B T} \right) d\xi \right]^N. \quad (47)$$

The FJC model prescribes rigid segments of fixed length ℓ .⁵⁶ In order to fix this length, we can consider the elastic constant $K \rightarrow +\infty$, and therefore we can apply the relationship

$e^{-\frac{K}{2k_B T}(\xi-\ell)^2} \rightarrow \sqrt{2\pi k_B T/K} \delta(\xi-\ell)$ (for $K \rightarrow +\infty$), where $\delta(\xi)$ is the Dirac delta function. Hence, the partition function converges to

$$Z_g(\eta) = \tilde{C}^N \left[\frac{\sinh\left(\frac{f\ell}{k_B T}\right)}{\frac{f\ell}{k_B T}} \right]^N = \tilde{C}^N \left(\frac{\sinh \eta}{\eta} \right)^N, \quad (48)$$

where $\eta = f\ell/(k_B T)$ is the normalized force, and \tilde{C} is a non-influential constant. This delivers the well-known force-extension relation

$$\langle r_N \rangle = k_B T \frac{\partial \log Z_g(f)}{\partial f} = N\ell \mathcal{L} \left(\frac{f\ell}{k_B T} \right) = N\ell \mathcal{L}(\eta), \quad (49)$$

where $r_N = \|\vec{r}_N\|$ and $\mathcal{L}(y) = \coth(y) - \frac{1}{y}$ is the Langevin function. We remark that while there is no purely elastic contribution in the FJC model since the connecting segments are rigid, the force-extension curve still exhibits elastic behavior. The elastic constant for low values of force can be written as $K_{\text{eff}} = \frac{3k_B T}{N\ell^2}$, which is proportional to the temperature T , and therefore the behavior is fully entropic. We will see that we can re-obtain the FJC model as a particular case of the three-dimensional daisy chain. Recent generalizations concern the freely jointed chain with reversible hinges,^{77,78} and the closed form expressions for the wormlike chain in the Gibbs and Helmholtz ensembles.⁷⁹

B. Thermoelastic model of a three-dimensional daisy chain

We first consider a daisy chain fluctuating in the three-dimensional space without additional rings. In this case, the potential $U(\xi)$ is zero in the interval $(0, \ell)$ (each ring can slide on the segment without experiencing forces), and is infinite for $\xi > \ell$ (the ring cannot go beyond the length of the segment, and its end then becomes an infinite energy barrier). Therefore, we deduce from Eq. (46) that the partition function for a daisy chain without rings is given by

$$Z_g(f) = C^N \left[\int_0^\ell \frac{\xi}{f} \sinh \left(\frac{f\xi}{k_B T} \right) d\xi \right]^N. \quad (50)$$

However, if we consider a three-dimensional daisy chain with the same structure of the system defined in Section II, the con-

tributions from the left and right rotaxane populations need to be added. By generalizing the one-dimensional result stated in Eq. (24), we obtain the complete partition function

$$Z_g(f) = C^N \left[\int_0^\ell \frac{\xi^n}{n!} \frac{(\ell-\xi)^m}{m!} \frac{\xi}{f} \sinh \left(\frac{f\xi}{k_B T} \right) d\xi \right]^N. \quad (51)$$

As before, adopting the change of variable $\xi = t\ell$, we get

$$Z_g(f) = C^N \left[\int_0^1 \frac{t^n \ell^n}{n!} \frac{\ell^m (1-t)^m}{m!} \frac{t\ell}{f} \sinh \left(\frac{ft\ell}{k_B T} \right) \ell dt \right]^N, \quad (52)$$

or, equivalently

$$Z_g(\eta) = \hat{C} \left[\int_0^1 t^{n+2} (1-t)^m \frac{\sinh(\eta t)}{\eta t} dt \right]^N, \quad (53)$$

where $\eta = \frac{f\ell}{k_B T}$ is the rescaled non-dimensional or normalized force, and \hat{C} is the new non-influential constant. This relation describes the behavior of the three-dimensional daisy chain represented in Fig. 7. We emphasize the similarity between the expressions for the one-dimensional case, Eq. (26), and for the three-dimensional case, Eq. (53). However, an important difference between the two partition functions lies in dependence on force term, with the presence of a hyperbolic sinc (sine cardinal) function $\frac{\sinh x}{x}$ in the three-dimensional case and an exponential function in the one-dimensional case. By using the classical thermodynamic relations,^{56,57} we can now determine the force-extension response

$$\begin{aligned} \langle r_N \rangle &= k_B T \frac{\partial \log Z_g(f)}{\partial f} = \ell \frac{\partial \log Z_g(\eta)}{\partial \eta} \\ &= N\ell \frac{\int_0^1 t^{n+2} (1-t)^m \frac{\partial}{\partial \eta} \frac{\sinh(\eta t)}{\eta t} dt}{\int_0^1 t^{n+2} (1-t)^m \frac{\sinh(\eta t)}{\eta t} dt}. \end{aligned} \quad (54)$$

Performing the internal derivative, we obtain

$$\langle r_N \rangle = N\ell \frac{\int_0^1 t^{n+2} (1-t)^m \frac{\eta t \cosh(\eta t) - \sinh(\eta t)}{\eta^2 t} dt}{\int_0^1 t^{n+2} (1-t)^m \frac{\sinh(\eta t)}{\eta t} dt}. \quad (55)$$

As already done in Section III A, a closed-form expression for $\langle r_N \rangle$ was calculated for easier implementation

$$\begin{aligned} \langle r_N \rangle &= -N\ell \frac{\sum_{j=0}^m \binom{m}{j} \frac{(n+j+1)!(n+j+3)}{\eta^{j+1}} \left[e^\eta \sum_{k=0}^{n+j+1} \frac{(-\eta)^k}{k!} + (-1)^{n+j+1} e^{-\eta} \sum_{k=0}^{n+j+1} \frac{\eta^k}{k!} - (1 + (-1)^{n+j+1}) \right]}{\sum_{j=0}^m \binom{m}{j} \frac{(n+j+1)!}{\eta^j} \left[e^\eta \sum_{k=0}^{n+j+1} \frac{(-\eta)^k}{k!} + (-1)^{n+j+1} e^{-\eta} \sum_{k=0}^{n+j+1} \frac{\eta^k}{k!} - (1 + (-1)^{n+j+1}) \right]}, \quad m \neq 0, \\ \langle r_N \rangle &= -N\ell \frac{2(-\eta)^n \sinh(\eta) + \frac{(n+1)!(n+3)}{\eta^2} \left[e^\eta \sum_{k=0}^{n+1} \frac{(-\eta)^k}{k!} + (-1)^{n+1} e^{-\eta} \sum_{k=0}^{n+1} \frac{\eta^k}{k!} - (1 + (-1)^{n+1}) \right]}{\frac{(n+1)!}{\eta} \left[e^\eta \sum_{k=0}^{n+1} \frac{(-\eta)^k}{k!} + (-1)^{n+1} e^{-\eta} \sum_{k=0}^{n+1} \frac{\eta^k}{k!} - (1 + (-1)^{n+1}) \right]}, \quad m = 0. \end{aligned} \quad (56)$$

We obtained these results with the same procedure discussed

in Appendix A for the one-dimensional case. These rela-

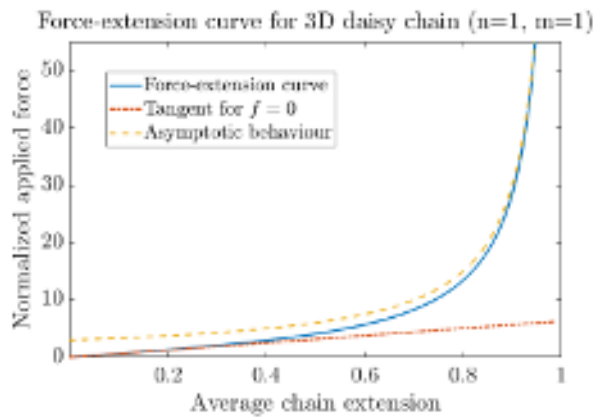


FIG. 8. Force-extension curve representing η versus $\frac{\langle r_N \rangle}{N\ell}$ for a three-dimensional daisy chain. In this example, we consider $n = 1$ and $m = 1$ and we also plot the tangent straight line in $\eta = 0$, see Eq. (60), and the asymptote for $\eta \rightarrow +\infty$, see Eq. (58). The equations for these limiting behaviors are given by $\eta = \frac{126}{20} \frac{k_B T}{N\ell^2} \langle r_N \rangle$, and $\eta = 3/(1 - \frac{\langle r_N \rangle}{N\ell})$, respectively.

tionships completely describe the nonlinear thermoelastic behavior of the three-dimensional daisy chain with an arbitrary number of rotaxanes in the two populations on the left and on the right with respect to the main sliding ring. As an example, with $n = m = 0$, we get

$$\langle r_N \rangle = N\ell \frac{3\eta \cosh \eta - 3 \sinh \eta - \eta^2 \sinh \eta}{\eta(\sinh \eta - \eta \cosh \eta)}, \quad (57)$$

which corresponds to the system in absence of rotaxanes, described by the partition function in Eq. (50).

Let us now consider two simple tests to assess the validity of this result ($\eta \simeq 0$ and $\eta \rightarrow +\infty$). Let us focus on the general case without external applied force ($f \simeq 0$, or, equivalently, $\eta \simeq 0$ for a force small compared to thermal fluctuations). For $\eta \simeq 0$, we have $\frac{\sinh(\eta z)}{\eta z} \simeq 1$, and $\frac{\eta t \cosh(\eta t) - \sinh(\eta t)}{\eta^2 t} \simeq \frac{1}{3} t^2 \eta$. Thus, Eq. (55), considering $\eta \simeq 0$, results in $\langle r_N \rangle \propto \eta$. This means that in absence of an applied force, the average value $\langle r_N \rangle$ is close to zero due to the isotropy of the system, coming from the spherical symmetry. As a consequence, since the free system can take the same configuration in all space directions, the average position of the free end is zero. Another noteworthy behavior of the system occurs when $\eta \rightarrow +\infty$ (i.e. $f \rightarrow +\infty$). In this case, from Eq. (56) we can obtain the asymptotic expression

$$\langle r_N \rangle \sim N\ell \left(1 - \frac{m+2}{\eta}\right) \underset{\eta \rightarrow +\infty}{\sim} N\ell. \quad (58)$$

Of course, when the force is very large, the system is quite perfectly aligned with the direction of the force and thus all the segments reach their maximum extension ℓ . The total length for large forces is therefore $N\ell$. As an example of application of these results, the force-extension curve for the case with $n = m = 1$ is displayed in Fig. 8. In this case the force-

extension relation is given by

$$\frac{\langle r_N \rangle}{N\ell} = \frac{(30 + 7\eta^2) \sinh \eta - (22 + \eta^2) \eta \cosh \eta - 8\eta}{\eta [4\eta \cosh \eta - (6 + \eta^2) \sinh \eta + 2\eta]}, \quad (59)$$

as obtained from Eq. (56). In Fig. 8, we also show the asymptotic behavior given by Eq. (58), and the tangent corresponding to the effective elastic constant defined for small values of the force (see below for the detailed analysis). We remark that the analysis based on asymptotic limits for small and large forces is typically performed for polymer chains such as FJC or WLC,⁸⁰ and this approach has been applied here to daisy chains.

C. Effective elastic constant of the three-dimensional daisy chain

Similarly to what was developed in Section III B, we deal with the determination of the elastic coefficient K_{eff} of the three-dimensional daisy chain as a function of n and m , i.e. the slope of the force-extension for $\eta = 0$: $1/K_{\text{eff}} = \frac{\partial \langle r_N \rangle}{\partial f} \Big|_{\eta \rightarrow 0}$. The mathematical details can be found in Appendix C, where we obtain this final result

$$K_{\text{eff}} = \frac{3k_B T}{N\ell^2} \frac{(n+m+5)(n+m+4)}{(n+4)(n+3)}. \quad (60)$$

Importantly, we note that $K_{\text{eff}} \sim \frac{3k_B T}{N\ell^2}$ when $n \rightarrow +\infty$ (with m fixed), which is exactly the value of the FJC model previously discussed. Indeed, when the number of rings at the left of each sliding segment becomes large, the configuration of the system is such that the extension of each element assumes the fixed length ℓ , because of the dominant effect of the left rotaxane gas. This explains the convergence to the FJC model. In this sense, the developed model appears to be a generalization of the FJC model. We also note that the expression for K_{eff} in the three-dimensional case is not symmetric with respect to n and m . This happens because of the spherical symmetry. In fact, the increase in force always results in a compression of the gas composed of m rotaxanes. Otherwise, a decrease in force creates more configurational freedom (or entropy) without necessarily resulting in a compression of the gas composed of n rotaxanes. This asymmetry can be also understood well by calculating the limit for $m \rightarrow +\infty$ (with n fixed), leading, e.g., to an effective constant $K_{\text{eff}} \simeq \frac{k_B T}{4N\ell^2} m^2$, when $n = 0$. Note that this quadratic behavior is completely different from the one observed in the one-dimensional case. This quadratic law can be used to design very stiff nano-springs but in this case they will also be very short, as will be discussed in the next Section. We also observe that when $n = m \rightarrow \infty$, we get the asymptotic behavior $K_{\text{eff}} \rightarrow \frac{12k_B T}{N\ell^2}$, similar to the FJC model, except for the constant. This expression is easily explained by observing that in the case where $n = m \rightarrow \infty$, the effective length of each segment becomes $\ell/2$. This is intuitive and follows strictly from Eq. (62) of the next Section. In any case, the expression

$K_{\text{eff}} \rightarrow \frac{12k_B T}{N\ell^2}$ comes therefore from the FJC result $K_{\text{eff}} = \frac{3k_B T}{N\ell^2}$, where we implement the substitution $\ell \rightarrow \ell/2$.

The effect of n and m on the thermoelastic response are graphically described in Fig. 9. In the top panel, we considered $m = 1$ and varied n . In this case we see that the elastic constant is always decreasing (slope of the curves in the origin). This can be deduced from our previous analysis of K_{eff} for small values of η . For large values of n the elastic constant converges to the characteristic value $K_{\text{eff}} = \frac{3k_B T}{N\ell^2}$ of the FJC model. In the central panel, we considered increasing values of $n = m$. In such a case we see that the elastic constant is always increasing and for large values of $n = m$ converges to the characteristic value $K_{\text{eff}} = \frac{12k_B T}{N\ell^2}$, previously discussed. In the bottom panel, we considered $n = 1$ and increasing values of m . In such a case we see that the elastic constant is strongly increasing with the law $K_{\text{eff}} = \frac{3k_B T}{20N\ell^2}(m+6)(m+5)$, which turns out to be quadratically unlimited for large values of m . We also observe that all top panel curves, in accordance with Eq. (58), have the same asymptotic behavior for large applied forces since m is constant. Differently, the curves of the other two panels have different asymptotic behaviors because the parameter m is variable, and thus it intervenes in Eq. (58).

D. Average length of each segment of the daisy chain

In addition to the force-extension relationship and the effective elastic constant, it is interesting to calculate the average value $\langle \xi \rangle$ of the distance between adjacent main rings in the daisy chain segments. Of course, this average value is independent of the segment considered since all elements are statistically independent, as previously discussed. From Eq. (51), it is not difficult to calculate the average value of ξ , and we find the expression

$$\begin{aligned} \langle \xi \rangle &= \frac{\int_0^\ell \frac{\xi^{n+1}}{n!} \frac{(\ell-\xi)^m}{m!} \frac{\xi}{f} \sinh\left(\frac{f\xi}{k_B T}\right) d\xi}{\int_0^\ell \frac{\xi^n}{n!} \frac{(\ell-\xi)^m}{m!} \frac{\xi}{f} \sinh\left(\frac{f\xi}{k_B T}\right) d\xi} \\ &= \ell \frac{\int_0^1 t^{n+3} (1-t)^m \frac{\sinh(\eta t)}{\eta t} dt}{\int_0^1 t^{n+2} (1-t)^m \frac{\sinh(\eta t)}{\eta t} dt}, \end{aligned} \quad (61)$$

where we used the substitution $\xi = t\ell$. While the full expression can be calculated by evaluating the integrals, it is now interesting to consider the average value of ξ when the system is free, that is, without applied forces ($\eta = 0$). In this case, we get

$$\begin{aligned} \langle \xi \rangle \Big|_{\eta=0} &= \ell \frac{\int_0^1 t^{n+3} (1-t)^m dt}{\int_0^1 t^{n+2} (1-t)^m dt} \\ &= \ell \frac{(n+3)!m!}{(n+m+4)!} \frac{(n+m+3)!}{(n+2)!m!} = \ell \frac{n+3}{n+m+4}. \end{aligned} \quad (62)$$

In accordance with our previous deductions, these results confirm that for $n \rightarrow +\infty$, each sliding segment will have a length ℓ (due to the effect of dominant left ring gas). Inversely, for $m \rightarrow +\infty$, the pressure exerted by the right ring gas reduces

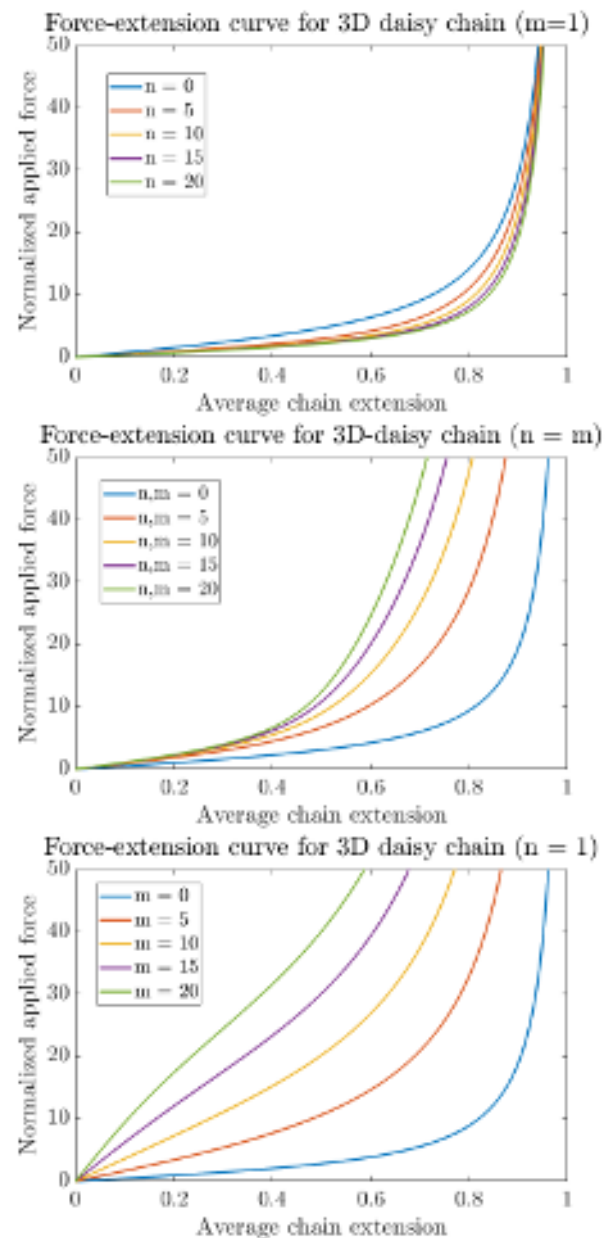


FIG. 9. Force-extension curve representing η versus $\frac{\langle r_N \rangle}{N\ell}$ for some three-dimensional daisy chains. In the top panel, we vary n while keeping $m = 1$. In the central panel, we vary $n = m$, and finally, in the bottom panel, we vary m with the fixed value $n = 1$.

the average length to zero. These mechanisms are now quite clear. However, a peculiar case arise when there are no rotaxane rings ($n = m = 0$), for which we obtain

$$\langle \xi \rangle \Big|_{\eta=0; n=m=0} = \frac{3}{4}\ell. \quad (63)$$

This result can be correctly interpreted as follows. In the one-dimensional case, we have obtained a similar result stating that $\langle x^i \rangle \Big|_{\eta=0} = \frac{\ell}{2}$ if $n = m$. It means that in the one-dimensional chain, the average length of the segment is $\frac{\ell}{2}$ when $n = m = 0$, without applied force. This symmetry is

intuitive for the one-dimensional case, in contrast to the asymmetry induced by the value $\frac{3}{4}\ell$ in the three-dimensional case, which therefore need to be further explained. To do this, we consider two adjacent points of the chain (corresponding to the main rings, in green in Fig. 7) and fix the first in the origin of the reference frame. We adopt spherical coordinates to deal with this problem. The second point is randomly distributed (with a uniform distribution) in a sphere of radius ℓ centered in the first point. This is true because the two rotaxanes gases are absent in this case. Hence, the goal now is to determine the average radius of a point randomly distributed in a sphere of radius ℓ . The probability density is uniform inside the sphere and therefore assumes the constant value $\frac{1}{\frac{4}{3}\pi\ell^3}$. Since the measure element in the sphere is given by $dx dy dz = \rho^2 \sin \theta d\theta d\phi d\xi$, we obtain

$$\langle \xi \rangle = \int_0^\ell \int_0^\pi \int_0^{2\pi} \frac{1}{\frac{4}{3}\pi\ell^3} \rho \rho^2 \sin \theta d\rho d\phi d\theta = \frac{3}{4}\ell, \quad (64)$$

which exactly corresponds to the value obtained for the chain. In conclusion, this means that the difference in the average value of the segment length, between one-dimensional and three-dimensional geometry, is due to spherical symmetry.

The generalization to the case where the segments are different from each other can be developed as described in Section III C, for the one-dimensional geometry. We do not report all the results here for the sake of brevity.

V. CONCLUSIONS

In this work, we proposed the design of a structure consisting of a daisy chain with additional rotaxane rings, aimed at creating entropic springs for a range of nanomechanical applications.

As a preliminary step, the origin of entropic forces is investigated for a one-dimensional system of rotaxane rings arranged along the same axis. For this simpler system, we demonstrated the origin of the pressure exerted by the gas of rings using both the Gibbs ensemble, at constant force, and the Helmholtz ensemble, at constant extension. Furthermore, we showed that these statistical ensembles are equivalent in the thermodynamic limit in this specific case.

The results obtained were then applied to the daisy chain model with additional loops. Specifically, two populations of rotaxanes were incorporated into each segment of the daisy chain, one to the left and the other to the right of the main sliding ring, respectively. These two populations exert opposing pressures on the main ring, significantly altering the system's elastic response. By selecting appropriate values for the number of rings in the left and right populations, the thermoelastic properties of the structure can be tailored to suit specific applications.

We analyzed the system in both the one-dimensional case, where the segments of the daisy chain are restricted to slide along a single direction, and the three-dimensional case, where the segments are free to move and rotate in three dimensions, as in the classical case of polymer models. In

both cases, we determined the nonlinear force-extension response, the effective elastic coefficient, and the behavior in the absence of applied force. These results are consistently expressed as functions of n and m , representing the number of rotaxanes in the left and right populations, respectively.

We found that the effective elastic coefficient is always a linear function of temperature, confirming that the phenomena described have a purely entropic origin. It is interesting to note that both the linear (effective elastic constant) and nonlinear behaviors can be finely tuned by adjusting the n and m parameters.

We highlighted significant differences in the behavior of one-dimensional and three-dimensional systems. First, we recovered the natural result that, in absence of applied external forces, the average value of the position of the free end in the three-dimensional case is always zero in the reference frame centered on the fixed end. This is due to the spherical symmetry of the system and contrasts with the one-dimensional case, where the average value is nonzero and depends on the system's structure.

Furthermore, the elastic constant is symmetric with respect to the parameters n and m in the one-dimensional case. However, this symmetry is broken in the three-dimensional case, once again due to the spherical symmetry of the system. In fact, compression and extension phenomena are symmetric in the one-dimensional case but lose this symmetry in the three-dimensional case. While extension can always be interpreted in the same way, compression behaves entirely differently in three dimensions due to the higher number of degrees of freedom and increased entropy. These factors allow for alternative configurations to pure compression.

The proposed structure can find applications in several directions, including artificial cytoskeletons, synthetic cells, and nano-mechanical logic gates. The development of artificial cells with specific programmable and tunable functions helps to explore the complex biological processes in natural cells with applications to medicine, environment, and the theory of the origin of life.^{81–84} In particular, one of the subsystems that must be recreated is the cytoskeleton, which has important mechanical functions in structuring and protecting the cellular environment.^{85–87} Therefore, the construction of synthetic cytoskeletons that mimic the features of their natural counterparts outlines a crucial step towards synthetic cells assembling. The proposed daisy chain scheme with rotaxanes is an excellent candidate for mimicking interlinking protein filaments constituting the cytoskeleton because of their linear and nonlinear mechanical versatility. Another interesting application concerns the developments of units for computation. We know that the linear processing of signals is not sufficient to perform logic operations. However, if we add to the set of linear operations any nonlinear function, the resulting set is able to perform digital computation.⁸⁸ This principle has been largely used to develop micro- and nano-mechanical devices able to implement logic gates.^{89–92} The elastic supramolecular elements introduced in this work can be used to develop logic gates, and their tunable nonlinearity is useful for optimizing their response in terms of signal stability.

Further prospects involve the generalization to cases where

the segments of the daisy chain exhibit bistable behavior,^{58,65} similar to that already studied and used in simpler rotaxanes. This could lead to better design of complex systems with phase transitions induced by temperature and applied forces.⁹³⁻⁹⁵ For the study of such systems, not only the equilibrium regime, as considered in this work, is of interest, but also the out-of-equilibrium regime including rate effects on the transitions between the two states of the bistable elements.⁹⁶⁻⁹⁸ Further perspectives may concern the two-dimensional case involving some additional mathematical difficulty because of the appearance of Bessel functions in the partition functions, or the case where there is damage in the structure induced by, for example, chain breaks or removal of links in segments of the structure.

ACKNOWLEDGMENTS

C.B., G.F. and G.P. have been supported by GNFM - Gruppo Nazionale per la Fisica Matematica (INdAM). G.F. and G.P.'s research is funded by the European Union (EU) - Next Generation EU. G.P. and G.F. are supported by PNRR, National Center for HPC, Big Data and Quantum Computing - M4C2 - I 1.4 (grant number CN00000013, CUP D93C22000430001) - Spoke 5 (Environment and Natural Disasters). G.P. and C.B. are supported by the Project of National Relevance (PRIN), financed by EU - Next-Generation EU - NRRP - M4C2 - I 1.1, CALL PRIN 2022 PNRR (Project P2022KHFNB, CUP D53D23018910001) granted by the Italian MUR. G.P. is supported by the PRIN, financed by EU - Next-Generation EU - NRRP - M4C2 - I 1.1, CALL PRIN 2022 (Project 2022XLBLRX, CUP D53D23006020006) granted by the Italian MUR. G.F. is supported by the PRIN, financed by EU - Next-Generation EU - NRRP - M4C2 - I 1.1, CALL PRIN 2022 PNRR (Project P2022MXCJ2, CUP D53D23018940001) and CALL PRIN 2022 (Project 2022MKB7MM, CUP D53D23005900006) granted by the Italian MUR. G.F. is also supported by "Istituto Nazionale di Fisica Nucleare" (INFN) through the project QUANTUM. S.G. and C.B. have been supported by "Central Lille" and "Région Hauts de France" under project StaMeNa (Statistical mechanics for macromolecular structures of nanotechnology). N.M.P. acknowledges the financial support of the European Union - Next Generation EU - National Recovery and Resilience Plan - NRRP - M4C2 - I 1.1, CALL PRIN 2022 D.D. 104/02-02-2022 - (PRIN2022 2022ATZCJN AMPHYBIA) CUP N. E53D23003040006. C.B. has been supported by "Université Franco Italienne" under the mobility grant VINCI 2024.

AUTHOR DECLARATIONS

Conflict of Interest

The authors have no conflicts to disclose.

Author Contributions

Gaétan Sanchez: Conceptualization (supporting); Formal analysis (equal); Investigation (equal); Methodology (equal); Writing – original draft (equal); Writing – review & editing (equal). **Claudia Binetti:** Conceptualization (supporting); Formal analysis (equal); Investigation (equal); Methodology (equal); Writing – original draft (equal); Writing – review & editing (equal). **Giuseppe Florio:** Conceptualization (lead); Formal analysis (equal); Investigation (equal); Methodology (equal); Supervision (equal); Writing – original draft (equal); Writing – review & editing (equal). **Nicola M. Pugno:** Conceptualization (lead); Formal analysis (equal); Investigation (equal); Methodology (equal); Supervision (equal); Writing – original draft (equal); Writing – review & editing (equal). **Giuseppe Puglisi:** Conceptualization (lead); Formal analysis (equal); Investigation (equal); Methodology (equal); Supervision (equal); Validation (equal); Writing – original draft (equal); Writing – review & editing (equal). **Stefano Giordano:** Conceptualization (lead); Formal analysis (equal); Funding acquisition (lead); Project administration (lead); Investigation (equal); Methodology (equal); Supervision (equal); Writing – original draft (equal); Writing – review & editing (equal).

DATA AVAILABILITY

The data that support the findings of this study are available from the corresponding author upon reasonable request.

Appendix A: Force-extension relation for the one-dimensional daisy chain

The force-extension relation for the one-dimensional daisy chain is given in Eq. (27). To obtain a closed form representation we first study the following integral

$$I_n = \int_0^a z^n e^{\eta z} dz. \quad (\text{A1})$$

By parts, we get

$$I_n = - \int_0^a n \frac{z^{n-1}}{\eta} e^{\eta z} dz + \frac{z^n}{\eta} e^{\eta z} \Big|_0^a = - \frac{n}{\eta} I_{n-1} + \frac{a^n}{\eta} e^{\eta a}, \quad (\text{A2})$$

and then we can obtain the final result recursively

$$I_n = \frac{n!}{(-1)^n \eta^{n+1}} \left[e^{a\eta} \sum_{k=0}^n \frac{(-a\eta)^k}{k!} - 1 \right]. \quad (\text{A3})$$

As an example, we can calculate I_0 , I_1 , and I_2 , as follows

$$I_0 = \frac{1}{\eta} (e^{\eta a} - 1), \quad (\text{A4})$$

$$I_1 = - \frac{1}{\eta^2} [e^{a\eta} (1 - a\eta) - 1], \quad (\text{A5})$$

$$I_2 = \frac{2}{\eta^3} \left[e^{a\eta} \left(1 - a\eta + \frac{a^2 \eta^2}{2} \right) - 1 \right]. \quad (\text{A6})$$

This result allows for the simplification of the partition function Z_g given in Eq. (26). By first using the binomial identity, we get

$$\begin{aligned} Z_g(f) &= C \left[\int_0^1 z^n (1-z)^m e^{\eta z} dz \right]^N \\ &= C \left[\int_0^1 z^n \sum_{h=0}^m \binom{m}{h} (-1)^h z^h e^{\eta z} dz \right]^N, \end{aligned} \quad (\text{A7})$$

and using Eq. (A3), we have

$$Z_g(f) = C \left[\sum_{h=0}^m (-1)^h \binom{m}{h} \frac{(n+h)!}{\eta^{n+h+1}} \left(e^{\eta} \sum_{k=0}^{n+h} \frac{(-\eta)^k}{k!} - 1 \right) \right]^N. \quad (\text{A8})$$

To conclude, we can implement the thermodynamic relation $\langle \tilde{x} \rangle = \ell \frac{\partial \log Z_g(\eta)}{\partial \eta}$, and we obtain Eq. (32) of the main text.

Appendix B: The elastic constant for the one-dimensional structure

The elastic constant of the one-dimensional daisy chain can be derived from the slope of the force-extension curve at the equilibrium point. Starting from Eq.(27), we first calculate the following derivative

$$\begin{aligned} \frac{\partial \langle \tilde{x} \rangle}{\partial f} &= \frac{\partial \langle \tilde{x} \rangle}{\partial \eta} \frac{\partial \eta}{\partial f} = \frac{N\ell^2}{k_B T} \frac{\partial}{\partial \eta} \frac{\int_0^1 t^{n+1} (1-t)^m e^{\eta t} dt}{\int_0^1 t^n (1-t)^m e^{\eta t} dt} \\ &= \frac{N\ell^2}{k_B T} \frac{\int_0^1 t^{n+2} (1-t)^m e^{\eta t} dt \int_0^1 t^n (1-t)^m e^{\eta t} dt}{\left[\int_0^1 t^n (1-t)^m e^{\eta t} dt \right]^2} \\ &\quad - \frac{N\ell^2}{k_B T} \frac{\left[\int_0^1 t^{n+1} (1-t)^m e^{\eta t} dt \right]^2}{\left[\int_0^1 t^n (1-t)^m e^{\eta t} dt \right]^2}. \end{aligned} \quad (\text{B1})$$

Now, for $\eta = 0$, we use the Beta functions and we get

$$\begin{aligned} \frac{\partial \langle \tilde{x} \rangle}{\partial f} \Big|_{f=0} &= \frac{N\ell^2}{k_B T} \frac{B(n+3, m+1)B(n+1, m+1)}{B^2(n+1, m+1)} \\ &\quad - \frac{N\ell^2}{k_B T} \frac{B^2(n+2, m+1)}{B^2(n+1, m+1)} \\ &= \frac{N\ell^2}{k_B T} \frac{(n+1)(m+1)}{(n+m+2)^2(n+m+3)}. \end{aligned} \quad (\text{B2})$$

We can therefore define the reciprocal effective elastic stiffness through the expression $1/K_{\text{eff}} = \frac{\partial \langle \tilde{x} \rangle}{\partial f} \Big|_{f=0}$, and we obtain the final result as

$$K_{\text{eff}} = \frac{k_B T}{N\ell^2} \frac{(n+m+2)^2(n+m+3)}{(n+1)(m+1)}. \quad (\text{B3})$$

This is the expression used in the main text.

Appendix C: The elastic constant for the three-dimensional structure

We determine the elastic constant for the three-dimensional structure, defined as the slope of the force-extension curve at the equilibrium point (i.e., for $\eta = 0$). First of all, by using Eq.(55) we have to elaborate the following derivative

$$\begin{aligned} \frac{\partial \langle r_N \rangle}{\partial f} &= \frac{N\ell^2}{k_B T} \frac{\int_0^1 t^{n+2} (1-t)^m F'' dt \int_0^1 t^{n+2} (1-t)^m F dt}{\left[\int_0^1 t^{n+2} (1-t)^m F dt \right]^2} \\ &\quad - \frac{N\ell^2}{k_B T} \frac{\left[\int_0^1 t^{n+2} (1-t)^m F' dt \right]^2}{\left[\int_0^1 t^{n+2} (1-t)^m F dt \right]^2}, \end{aligned} \quad (\text{C1})$$

where we introduced

$$\begin{aligned} F &= \frac{\sinh(\eta t)}{\eta t}, \\ F' &= \frac{\partial F}{\partial \eta} = \frac{\eta t \cosh(\eta t) - \sinh(\eta t)}{\eta^2 t}, \\ F'' &= \frac{\partial^2 F}{\partial \eta^2} = \frac{\eta t \sinh(\eta t)}{\eta} - 2 \frac{\eta t \cosh(\eta t) - \sinh(\eta t)}{\eta^3 t}. \end{aligned} \quad (\text{C2})$$

For $\eta \simeq 0$, these quantities read $F \simeq 1$, $F' \simeq 0$, and $F'' \simeq \frac{1}{3}t^2$. Therefore, we can write

$$\begin{aligned} \frac{\partial \langle r_N \rangle}{\partial f} \Big|_{\eta \rightarrow 0} &= \frac{N\ell^2}{3k_B T} \frac{\int_0^1 t^{n+4} (1-t)^m dt}{\int_0^1 t^{n+2} (1-t)^m dt} \\ &= \frac{N\ell^2}{3k_B T} \frac{B(n+5, m+1)}{B(n+3, m+1)} \\ &= \frac{N\ell^2}{3k_B T} \frac{(n+4)(n+3)}{(n+m+5)(n+m+4)}. \end{aligned} \quad (\text{C3})$$

This leads to the definition of the inverse effective elastic coefficient for $\eta \rightarrow 0$ as $1/K_{\text{eff}} = \frac{\partial \langle r_N \rangle}{\partial f} \Big|_{\eta \rightarrow 0}$, leading to this final result

$$K_{\text{eff}} = \frac{3k_B T}{N\ell^2} \frac{(n+m+5)(n+m+4)}{(n+4)(n+3)}, \quad (\text{C4})$$

corresponding to the expression used in the main text.

¹L. Fang, M. A. Olson, D. Benitez, E. Tkatchouk, W. A. G. IIIb, and J. F. Stoddart, "Mechanically bonded macromolecules," *Chemical Society Reviews* **39**, 17–29 (2010).

²J. Rotzler and M. Mayor, "Molecular daisy chains," *Chem. Soc. Rev.* **42**, 44–62 (2013).

³Q. Wu, P. M. Rauscher, X. Lang, R. J. Wojtecki, J. J. de Pablo, M. J. A. Hore, and S. J. Rowan, "Poly[n]catenanes: Synthesis of molecular interlocked chains," *Science* **358**, 1434–1439 (2017).

⁴L. F. Hart, J. E. Hertzog, P. M. Rauscher, B. W. Rawe, M. M. Tranquilli, and S. J. Rowan, "Material properties and applications of mechanically interlocked polymers," *Nat. Rev. Mater.* **6**, 508–530 (2021).

⁵L. Tubiana, G. P. Alexander, A. Barbensi, D. Buck, J. Cartwright, M. Chwastyk, M. Cieplak, I. Coluzza, S. Čopar, D. J. Craik, M. D. Stefano, R. Everaers, P. F. Faísca, F. Ferrari, A. Giacometti, D. Goundaroulis, E. Haglund, Y.-M. Hou, N. Ilieva, S. E. Jackson, A. Japaridze, N. Kaplan, A. R. Klotz, H. Li, C. N. Likos, E. Locatelli, T. López-León, T. Machon,

- C. Micheletti, D. Michieletto, A. Niemi, W. Niemyska, S. Niewieczerzal, F. Nitti, E. Orlandini, S. Pasquali, A. P. Perlinska, R. Podgornik, R. Potesio, N. M. Pugno, M. Ravnik, R. Ricca, C. M. Rohwer, A. Rosa, J. Smrek, A. Souslov, A. Stasiak, D. Steer, J. Sułkowska, P. Sułkowski, D. W. L. Sumners, C. Svaneborg, P. Szymczak, T. Tarenzi, R. Travasso, P. Virnau, D. Vlassopoulos, P. Zihler, and S. Žumer, "Topology in soft and biological matter," *Physics Reports* **1075**, 1–137 (2024).
- ⁶J.-M. Lehn, "Supramolecular chemistry," *Science* **260**, 1762–1763 (1993).
- ⁷H.-J. Schneider, "Binding mechanisms in supramolecular complexes," *Angew. Chem. Int. Ed.* **48**, 3924–3977 (2009).
- ⁸F. Biedermann and H.-J. Schneider, "Experimental binding energies in supramolecular complexes," *Chem. Rev.* **116**, 5216–5300 (2016).
- ⁹Y. Jiao, X.-Y. Chen, and J. F. Stoddart, "Weak bonding strategies for achieving regio- and site-selective transformations," *Chem.* **8**, 414–438 (2022).
- ¹⁰J. Fischer and M. Wendland, "On the history of key empirical intermolecular potentials," *Fluid Phase Equilibria* **573**, 113876 (2023).
- ¹¹L. Fabbrizzi, *Beauty in Chemistry. Artistry in the Creation of New Molecules* (Springer-Verlag, Berlin, 2012).
- ¹²V. H. J. Frey, T. Kraus and J.-P. Sauvage, "A catenane consisting of a large ring threaded through both cyclic units of a handcuff-like compound," *Chem. Commun.* **2005**, 5310–5312 (2005).
- ¹³L. Tubiana, F. Ferrari, and E. Orlandini, "Circular polycatenanes: Supramolecular structures with topologically tunable properties," *Phys. Rev. Lett.* **129**, 227801 (2022).
- ¹⁴T. Takata, "Polyrotaxane and polyrotaxane network: Supramolecular architectures based on the concept of dynamic covalent bond chemistry," *Polym. J.* **38**, 1–20 (2006).
- ¹⁵R. E. Fadler and A. H. Flood, "Rigidity and flexibility in rotaxanes and their relatives; on being stubborn and easy-going," *Frontiers in Chemistry* **10**, 856173 (2022).
- ¹⁶A. Saura-Sanmartin, "Synthesis of 'impossible' rotaxanes," *Chemistry – A European Journal* **30**, e202304025 (2024).
- ¹⁷S. Nygaard, K. Leung, I. Aprahamian, T. Ikeda, S. Saha, B. Laursen, S.-Y. Kim, S. Hansen, P. Stein, A. Flood, J. Stoddart, and J. Jeppesen, "Functionally rigid bistable [2]rotaxanes," *Journal of the American Chemical Society* **129**, 960–70 (2007).
- ¹⁸T. Ye, A. S. Kumar, S. Saha, T. Takami, T. J. Huang, J. F. Stoddart, and P. S. Weiss, "Changing stations in single bistable rotaxane molecules under electrochemical control," *ACS nano* **4**, 3697–3701 (2010).
- ¹⁹A. C. Fahrenbach, J. C. Barnes, H. Li, D. Benítez, A. N. Basuray, L. Fang, C.-H. Sue, G. Barin, S. K. Dey, W. A. Goddard III, and J. F. Stoddart, "Measurement of the ground-state distributions in bistable mechanically interlocked molecules using slow scan rate cyclic voltammetry," *Proceedings of the National Academy of Sciences* **108**, 20416–20421 (2011).
- ²⁰Y. Liu, Q. Zhang, W.-H. Jin, T.-Y. Xu, D.-H. Qu, and H. Tian, "Bistable [2]rotaxane encoding an orthogonally tunable fluorescent molecular system including white-light emission," *Chemical Communications* **54**, 10642–10645 (2018).
- ²¹P. R. Ashton, I. W. Parsons, F. M. Raymo, J. F. Stoddart, A. J. P. White, D. J. Williams, and R. Wolf, "Self-assembling supramolecular daisy chains," *Angewandte Chemie International Edition* **37**, 1913–1916 (1998).
- ²²K. Fournel-Marotte and F. Coutrot, "Moving into another dimension," *Nature Chemistry* **9**, 105–106 (2017).
- ²³J.-C. Chang, S.-H. Tseng, C.-C. Lai, Y.-H. Liu, S.-M. Peng, and S.-H. Chiu, "Mechanically interlocked daisy-chain-like structures as multidimensional molecular muscles," *Nature Chemistry* **9**, 128–134 (2016).
- ²⁴A. Goujon, T. Lang, G. Mariani, E. Moulin, G. Fuks, J. Raya, E. Buhler, and N. Giuseppone, "Bistable [c2]daisy chain rotaxanes as reversible muscle-like actuators in mechanically active gels," *Journal of the American Chemical Society* **139**, 14825–14828 (2017).
- ²⁵A. Goujon, E. Moulin, G. Fuks, and N. Giuseppone, "[c2]daisy chain rotaxanes as molecular muscles," *CCS Chemistry* **1**, 83–96 (2019).
- ²⁶A. Caballero, F. Zapata, and P. D. Beer, "Interlocked host molecules for anion recognition and sensing," *Coordination Chemistry Reviews* **257**, 2434–2455 (2013).
- ²⁷S. F. M. van Dongen, S. Cantekin, J. A. A. W. Elemans, A. E. Rowan, and R. J. M. Nolte, "Functional interlocked systems," *Chem. Soc. Rev.* **43**, 99–122 (2014).
- ²⁸T. J. Huang, A. H. Flood, B. Brough, Y. Liu, P. A. Bonvallet, S. Kang, C.-W. Chu, T.-F. Guo, W. Lu, Y. Yang, J. F. Stoddart, and C.-M. Ho, "Understanding and harnessing biomimetic molecular machines for NEMS actuation materials," *IEEE Transactions on Automation Science and Engineering* **3**, 254–259 (2006).
- ²⁹I. Aprahamian, "The future of molecular machines," *ACS Central Science* **6**, 347–358 (2020).
- ³⁰A. K. Rajendran, Y. Arisaka, N. Yui, and S. Iseki, "Polyrotaxanes as emerging biomaterials for tissue engineering applications: a brief review," *Inflammation and Regeneration* (2020).
- ³¹J. Riebe and J. Niemeyer, "Mechanically interlocked molecules for biomedical applications," *European Journal of Organic Chemistry* **2021**, 5106–5116 (2021).
- ³²H. Kim, W. A. Goddard III, S. S. Jang, W. R. Dichtel, J. R. Heath, and J. F. Stoddart, "Free energy barrier for molecular motions in bistable [2]rotaxane molecular electronic devices," *The Journal of Physical Chemistry A* **113**, 2136–2143 (2009).
- ³³P. Wu, B. Dharmadhikari, P. K. Patra, and X. Xiong, "Rotaxane nanomachines in future molecular electronics," *Nanoscale Advances* **4**, 3418–3461 (2022).
- ³⁴C. Schäfer, G. Ragazzon, B. Colasson, M. La Rosa, S. Silvi, and A. Credi, "An artificial molecular transporter," *ChemistryOpen* **5**, 120–124 (2016).
- ³⁵L. Chen, R. Nixon, and G. D. Bo, "Force-controlled release of small molecules with a rotaxane actuator," *Nature* **628**, 320–325 (2024).
- ³⁶A. Tanaka, K. Kato, K. Ito, and K. Urayama, "Pronounced effects of the densities of threaded rings on the strain-dependent poisson's ratio of polyrotaxane gels with movable cross-links," *Soft matter* **14**, 2808–2815 (2018).
- ³⁷Z. Zhang, W. You, P. Li, J. Zhao, Z. Guo, T. Xu, J. Chen, W. Yu, and X. Yan, "Insights into the correlation of microscopic motions of [c2]daisy chains with macroscopic mechanical performance for mechanically interlocked networks," *Journal of the American Chemical Society* **145**, 567–578 (2022).
- ³⁸S.-W. Zhou, D. Zhou, R. Gu, C.-S. Ma, C. Yu, and D.-H. Qu, "Mechanically interlocked [c2]daisy chain backbone enabling advanced shape-memory polymeric materials," *Nature Communications* **15**, 1690 (2024).
- ³⁹P. Wei, X. Yan, and F. Huang, "Supramolecular polymers constructed by orthogonal self-assembly based on host-guest and metal-ligand interactions," *Chemical Society Reviews* **44**, 815–832 (2015).
- ⁴⁰H. Han, J. S. W. Seale, L. Feng, Y. Qiu, and J. F. Stoddart, "Sequence-controlled synthesis of rotaxanes," *Journal of Polymer Science* **61**, 881–902 (2023).
- ⁴¹S. J. Cantrill, S. J. Rowan, and J. F. Stoddart, "Rotaxane formation under thermodynamic control," *Organic Letters* **1**, 1363–1366 (1999).
- ⁴²A. Dunlop, J. Wattoom, E. A. Hasan, T. Cosgrove, and A. N. Round, "Mapping the positions of beads on a string: dethreading rotaxanes by molecular force spectroscopy," *Nanotechnology* **19**, 345706 (2008).
- ⁴³P. Lussis, T. Svaldo-Lanero, A. Bertocco, C.-A. Fustin, D. A. Leigh, and A.-S. Duwez, "A single synthetic small molecule that generates force against a load," *Nature Nanotechnology* **6**, 553–557 (2011).
- ⁴⁴D. Sluysmans, F. Devaux, C. J. Bruns, J. F. Stoddart, and A.-S. Duwez, "Dynamic force spectroscopy of synthetic oligorotaxane foldamers," *Proceedings of the National Academy of Sciences* **115**, 9362–9366 (2018).
- ⁴⁵D. Sluysmans, P. Lussis, C.-A. Fustin, A. Bertocco, D. A. Leigh, and A.-S. Duwez, "Real-time fluctuations in single-molecule rotaxane experiments reveal an intermediate weak binding state during shuttling," *J. Am. Chem. Soc.* **143**, 2348–2352 (2021).
- ⁴⁶R. J. J. Boesten, E. M. Sevick, and D. R. M. Williams, "Piston rotaxane monolayers: shear swelling and nanovalve behavior," *Macromolecules* **43**, 7244–7249 (2010).
- ⁴⁷E. M. Sevick and D. R. M. Williams, "Piston-rotaxanes as molecular shock absorbers," *Langmuir* **26**, 5864–5868 (2010).
- ⁴⁸E. M. Sevick and D. R. M. Williams, "A piston-rotaxane with two potential stripes: Force transitions and yield stresses," *Molecules* **18**, 13398–13409 (2013).
- ⁴⁹E. M. Sevick and D. R. M. Williams, "A two-stroke, two-cylinder piston rotaxane motor," *ChemPhysChem* **17**, 1927–1933 (2016).
- ⁵⁰E. M. Sevick and D. R. M. Williams, "Conformational isomers of linear rotaxanes," *The Journal of Chemical Physics* **141**, 114904 (2014).
- ⁵¹E. M. Sevick and D. R. M. Williams, "Threading a ring or tube onto a rod: An entropically rare event," *Nano Letters* **16**, 671–674 (2015).

- ⁵²T. C. Harris, E. M. Sevick, and D. R. M. Williams, “Mechanical conformers of keyring catenanes,” *The Journal of Physical Chemistry A* **122**, 8923–8930 (2018).
- ⁵³P. Reddy, E. M. Sevick, and D. R. M. Williams, “Triangular cyclic rotaxanes: Size, fluctuations, and switching properties,” *Proceedings of the National Academy of Sciences* **115**, 9367–9372 (2018).
- ⁵⁴H. He, E. M. Sevick, and D. R. M. Williams, “Rotaxane liquid crystals with variable length: The effect of switching efficiency on the isotropic-nematic transition,” *J. Chem. Phys.* **148**, 134905 (2018).
- ⁵⁵J. W. Gibbs, *Elementary principles in statistical mechanics: developed with especial reference to the rational foundations of thermodynamics* (C. Scribner’s sons, 1902).
- ⁵⁶J. H. Weiner, *Statistical mechanics of elasticity* (Dover Publications, New York, 1983).
- ⁵⁷F. Manca, S. Giordano, P. L. Palla, R. Zucca, F. Cleri, and L. Colombo, “Elasticity of flexible and semiflexible polymers with extensible bonds in the Gibbs and Helmholtz ensembles,” *J. Chem. Phys.* **136**, 154906 (2012).
- ⁵⁸M. Benedito and S. Giordano, “Thermodynamics of small systems with conformational transitions: The case of two-state freely jointed chains with extensible units,” *J. Chem. Phys.* **149**, 054901 (2018).
- ⁵⁹B. Bianco, E. Moggia, S. Giordano, W. Rocchia, and A. Chiabrera, “Friction and noise in quantum mechanics: A model for the interactions between a system and a thermal bath,” *Nuovo Cim. B* **116**, 155–167 (2001).
- ⁶⁰F. Manca, P.-M. Déjardin, and S. Giordano, “Statistical mechanics of holonomic systems as a brownian motion on smooth manifolds,” *Ann. Phys.* **528**, 381–393 (2016).
- ⁶¹S. Giordano, “Stochastic thermodynamics of holonomic systems,” *Eur. Phys. J. B* **92**, 174 (2019).
- ⁶²P. Stein, “A note on the volume of a simplex,” *The American Mathematical Monthly* **73**, 299–301 (1966).
- ⁶³R. G. Winkler, “Equivalence of statistical ensembles in stretching single flexible polymers,” *Soft Matter* **6**, 183–6191 (2010).
- ⁶⁴F. Manca, S. Giordano, P. L. Palla, F. Cleri, and L. Colombo, “On the equivalence of thermodynamics ensembles for flexible polymer chains,” *Phys. A: Stat. Mech. Appl.* **395**, 154–170 (2014).
- ⁶⁵S. Giordano, “Spin variable approach for the statistical mechanics of folding and unfolding chains,” *Soft Matter* **13**, 6877 (2017).
- ⁶⁶S. Giordano, “Helmholtz and Gibbs ensembles, thermodynamic limit and bistability in polymer lattice models,” *Continuum Mechanics and Thermodynamics* **30**, 459–483 (2018).
- ⁶⁷L. Bellino, G. Florio, and G. Puglisi, “The influence of device handles in single-molecule experiments,” *Soft Matter* **15**, 8680 (2019).
- ⁶⁸G. Florio and G. Puglisi, “Unveiling the influence of device stiffness in single macromolecule unfolding,” *Sci. Rep.* **9**, 4997 (2019).
- ⁶⁹S. Dutta and P. Benetatos, “Inequivalence of fixed-force and fixed-extension statistical ensembles for a flexible polymer tethered to a planar substrate,” *Soft Matter* **14**, 6857–6866 (2018).
- ⁷⁰S. Dutta and P. Benetatos, “Statistical ensemble inequivalence for flexible polymers under confinement in various geometries,” *Soft Matter* **16**, 2114–2127 (2020).
- ⁷¹P. Benetatos, “Ensemble inequivalence and negative extensibility in a strongly stretched wormlike chain with fluctuating bending stiffness,” *J. Chem. Phys.* **157**, 164112 (2022).
- ⁷²D. I. Dimitrov, L. I. Klushin, A. M. Skvortsov, A. Milchev, and K. Binder, “The escape transition of a polymer: A unique case of non-equivalence between statistical ensembles,” *Eur. Phys. J. E* **29**, 9–25 (2009).
- ⁷³A. M. Skvortsov, L. I. Klushin, A. A. Polotsy, and K. Binder, “Mechanical desorption of a single chain: Unusual aspects of phase coexistence at a first-order transition,” *Phys. Rev. E* **85**, 031803 (2012).
- ⁷⁴G. Florio, S. Giordano, and G. Puglisi, “Continuum vs thermodynamical limit in statistical mechanics,” Submitted (2025).
- ⁷⁵I. S. Gradshteyn and I. M. Ryzhik, *Table of Integrals, Series and Products* (Academic Press, San Diego, 1965).
- ⁷⁶M. Abramowitz and I. A. Stegun, *Handbook of Mathematical Functions* (Dover Publications, New York, 1970).
- ⁷⁷G. Noh and P. Benetatos, “Tensile elasticity of a freely jointed chain with reversible hinges,” *Soft Matter* **17**, 3333–3345 (2021).
- ⁷⁸M. Yi, D. Lee, and P. Benetatos, “Bending elasticity of the reversible freely jointed chain,” *Journal of Chemical Physics* **161**, 234908 (2024).
- ⁷⁹N. T. Andersen and J. Z. Y. Chen, “Forced extension of a wormlike chain in the Gibbs and Helmholtz ensembles,” *Journal of Chemical Physics* **160**, 084903 (2024).
- ⁸⁰F. Manca, S. Giordano, P. L. Palla, F. Cleri, and L. Colombo, “Theory and Monte Carlo simulations for the stretching of flexible and semiflexible single polymer chains under external fields,” *J. Chem. Phys.* **137**, 244907 (2012).
- ⁸¹C. Xu, S. Hu, and X. Chen, “Artificial cells: from basic science to applications,” *Materials Today* **19**, 516–532 (2016).
- ⁸²K. Liu, J. Yang, S. Ding, and Y. Gao, “Daisy chain topology based mammalian synthetic circuits for RNA-only delivery,” *ACS Synth. Biol.* **9**, 269–282 (2020).
- ⁸³Y. Lu, G. Allegri, and J. Huskens, “Vesicle-based artificial cells: materials, construction methods and applications,” *Materials Horizons* **9**, 892–907 (2022).
- ⁸⁴B. Ghosh, “Artificial cell design: reconstructing biology for life science applications,” *Emerging Topics in Life Sciences* **6**, 619–627 (2022).
- ⁸⁵K. A. Ganar, L. W. Honaker, and S. Deshpande, “Shaping synthetic cells through cytoskeleton-condensate-membrane interactions,” *Current Opinion in Colloid & Interface Science* **54**, 101459 (2021).
- ⁸⁶P. Zhan, K. Jahnke, N. Liu, and K. Göpfrich, “Functional dna-based cytoskeletons for synthetic cells,” *Nature Chemistry* **14**, 958–963 (2022).
- ⁸⁷D. Sauter, M. Schröter, C. Frey, C. Weber, U. Mersdorf, J.-W. Janiesch, I. Platzman, and J. P. Spatz, “Artificial cytoskeleton assembly for synthetic cell motility,” *Macromolecular Bioscience* **23**, 2200437 (2023).
- ⁸⁸S. Lloyd, “Any nonlinear gate, with linear gates, suffices for computation,” *Physics Letters A* **167**, 255–260 (1992).
- ⁸⁹Y. Song, R. M. Panas, S. Chizari, L. A. Shaw, J. A. Jackson, J. B. Hopkins, and A. J. Pascall, “Additively manufacturable micro-mechanical logic gates,” *Nature Communications* **10**, 882 (2019).
- ⁹⁰U. Waheed, C. Myant, and S. Dobson, “Boolean and/or mechanical logic using multi-plane mechanical metamaterials,” *Extreme Mechanics Letters* **40**, 100865 (2020).
- ⁹¹L. Wu and D. Pasini, “In situ activation of snap-through instability in multi-response metamaterials through multistable topological transformation,” *Advanced Materials* **35**, 2301109 (2023).
- ⁹²X. Hou, T. Sheng, F. Xie, and Z. Deng, “Mechanical logic gate design based on multi-stable metamaterial with multi-step deformation,” *Composite Structures* **335**, 118001 (2024).
- ⁹³A. Prados, A. Carpio, and L. L. Bonilla, “Sawtooth patterns in force-extension curves of biomolecules: An equilibrium-statistical-mechanics theory,” *Phys. Rev. E* **88**, 012704 (2013).
- ⁹⁴L. L. Bonilla, A. Carpio, and A. Prados, “Theory of force-extension curves for modular proteins and DNA hairpins,” *Phys. Rev. E* **91**, 052712 (2015).
- ⁹⁵A. Cannizzo, L. Bellino, G. Florio, G. Puglisi, and S. Giordano, “Thermal control of nucleation and propagation transition stresses in discrete lattices with non-local interactions and non-convex energy,” *Eur. Phys. J. Plus* **137**, 569 (2022).
- ⁹⁶I. Benichou and S. Givli, “Rate dependent response of nanoscale structures having a multiwell energy landscape,” *Phys. Rev. Lett.* **114**, 095504 (2015).
- ⁹⁷I. Benichou, Y. Zhang, O. K. Dudko, and S. Givli, “The rate dependent response of a bistable chain at finite temperature,” *Journal of the Mechanics and Physics of Solids* **95**, 44–63 (2016).
- ⁹⁸A. Cannizzo and S. Giordano, “Statistical mechanics approaches for studying temperature and rate effects in multistable systems,” *Symmetry* **16**, 632 (2024).